R. & M. No. 3763

PROCUREMENT EXECUTIVE, MINISTRY OF DEFENCE

AERONAUTICAL RESEARCH COUNCIL
REPORTS AND MEMORANDA

Measurements in Low-speed Flow of Unsteady Pressure Distributions on a Rectangular Wing with an Oscillating Control Surface

BY D. A. DRANE

Structures Dept., R.A.E., Farnborough

LONDON: HER MAJESTY'S STATIONERY OFFICE

1976

£3.50 NET

Measurements in Low-speed Flow of Unsteady Pressure Distributions on a Rectangular Wing with an Oscillating Control Surface

By D. A. Drane

Structures Department, R.A.E., Farnborough

Reports and Memoranda No. 3763*
October, 1970

Summary

The report describes an experiment made jointly by an Anglo-French team to determine unsteady pressure distributions and forces on a low aspect ratio wing with an oscillating control surface. Two series of tests were made in the R.A.E. 5 ft low-speed wind tunnel at frequency parameters between 0·73 and 8·45. The pressure-measuring installations were of two types; one consisted of a number of individual transducers, and the other employed a series of tubes connected to a single transducer via a pressure switch. The results were compared with calculations based on methods developed at R.A.E. and O.N.E.R.A.

The tests showed that the measuring systems provided results which were in themselves consistent; there were, however, disparities between upper and lower surface oscillatory pressure distributions which made comparisons between theory and experiment difficult.

* Replaces R.A.E. Technical Reports 70182 and 71113—A.R.C. 33 080 and A.R.C. 33 515.

LIST OF CONTENTS

1. Introduction

In 1968 an Anglo-French research panel was set up to discuss, and where possible co-ordinate, research into problems of flutter and unsteady aerodynamics which were of mutual interest. One result was a decision by the panel to make a joint investigation of the unsteady pressure distributions over wings with oscillating control surfaces in low- and high-speed flow. The present report covers an investigation in low-speed flow at low, moderate and high frequency parameters for which O.N.E.R.A. provided the model and some instrumentation and R.A.E. provided wind-tunnel facilities and further instrumentation. The tests were made by a combined Anglo-French team.

The main object of the experiment was to measure the unsteady pressure distributions induced on a rectangular wing of low aspect ratio by small-amplitude sinusoidal perturbations of the control surfaces, and to compare the results with theory. A subsidiary object of the experiment was to gain experience of systems for measuring very small unsteady pressures. Two control surfaces, having the same chord but differing in span, were tested at low, moderate and high frequency parameters and at mean incidence settings of $\pm 3{\cdot}5$ and 0 degrees. The unsteady pressure distributions were measured by two independent systems. The first was of the type pioneered by Bergh;[1] in this sytem a single transducer is connected to a number of pressure tappings in turn via a pressure switch. The second system, used only during the first phase of the tests, consisted of a series of individual pressure transducers. Unsteady pressure distributions for both configurations were calculated by the methods of Garner et al,[2,3] Long[4] and Dat et al.[5,6]

Within the limitations of the present experiment the theoretical distributions were in acceptable agreement with each other, and followed the trends set by the experiments. It was not possible, however, to establish any general quantitative relationship between theory and experiment in the investigation because of the disparities between unsteady pressure distributions measured on upper and lower surfaces. The measurements themselves followed the general patterns set by calculation, but further work would be needed to resolve the discrepancies between distributions.

2. Apparatus and Method of Test

2.1. Model

The model (Figs. 1 and 2) consisted of two rectangular half-wings (N.A.C.A. 64A section) of 6 per cent thickness/chord ratio with a net aspect ratio of 1·25. Each half-wing was cantilevered from a vertical flat plate with a sharp leading edge. The two plates (Fig. 3) were parallel to each other and all the excitation and measuring equipment was installed between them in a nacelle with an aerofoil section of 9 per cent thickness/chord ratio. The nacelle was located eccentrically with respect to the plane of the wings—*see* Fig. 3. The control surfaces were hinged by cross-springs along an axis at the two-thirds chord line.

Wings and controls were constructed in the same way; both consisted of a skeleton framework of ribs and spars milled from a solid aluminium alloy plate to which top and bottom skins were attached by screws. In each control surface there were two frameworks; the outer span portion could be fixed by attaching appropriate skins either to the main wing (so providing an inboard 60 per cent span control) or it could be connected to the inner portion of the control surface (so providing a full-span control). The hinge stiffnesses were controlled by springs in the nacelle. Oscillatory pressures were measured by tapping from holes drilled through perspex inserts set in the model (Fig. 4). By blanking off one end of the insert with thin adhesive tape, pressures could be measured on either upper or lower surfaces.

2.2. Support System

Each half-wing was attached to the central nacelle by a three-component strain-gauged balance. The wings and central plates were fixed to a steel framework which was insulated from the tunnel structure by rubber anti-vibration mountings. The whole rig was assembled in the working section of the R.A.E. 5 ft open-jet wind tunnel.

2.3. Excitation

The control surfaces were vibrated at resonance by two moving coil exciters attached to one end of a rocker arm (Fig. 5); at the other end of this arm were two coil springs which determined the structural hinge stiffness. The static deflection of the control could be altered between 0 and 5 degrees by changing the datum of the springs; three sets of springs were available giving wind-off resonance frequencies of approximately 15, 24 and 31 Hz.

2.4. Instrumentation

Two separate systems were used to measure the oscillatory pressures. The first consisted of 36 Telco miniature pressure transducers installed mainly in the inboard starboard control surface. The second pressure measurement system employed a single Statham PL31 transducer to sense pressures from 47 separate channels on the port side via a Scanivalve pressure switch. The tubes were installed in the wing and outboard control surface. Between the pressure tappings and the Scanivalve they were geometrically similar; that is to say they had the same type of attachment, the same length and the same diameter. One channel furnished a continuous dynamic reference-pressure signal. The presence of the tubes affected the amplitude and phase response of the pressure recorded by the transducer and it was therefore necessary to apply a complex frequency-dependent correction factor to the recorded results.[1]

The individual transducers gave results which were subject to greater scatter than those from the pressure-switch system. The miniature pressure transducers were therefore removed before the second phase of testing was begun and replaced by a second pressure-switch system. At the same time some additional pressure tappings were made in the starboard wing. Fig. 4 shows the locations at which pressures were measured.

Forces on the model were obtained by measurements from the strain-gauge balances. There were four readings of bending moment and two of torsion; lift forces were deduced by differencing the bending-moment readings. To obtain real parts of the aerodynamic values it was necessary to subtract the inertia forces and rocker-arm reaction loads.

2.5. Recording

Two sets of recording equipment were available. In the O.N.E.R.A. system the signals furnished by the transducers were fed into a measuring system composed of multiplying and integrating circuits; after a correction had been inserted for the transfer function of the tubes, these provided in-phase and in-quadrature components of the pressures relative to the movement of the control. The period of integration could be varied but was most frequently chosen to be five seconds. The integrated values were read on a digital voltmeter and printed out on the channels of a data-logging system; one pair of readings could be processed whilst a second pair was being taken. The linearity of the integration was monitored on a storage oscilloscope.

The system provided by R.A.E. (the Elvira equipment)[7] differed in that the input was continuously averaged. It was slower because it handled only one channel at a time. This system was used for the series of measurements made at moderate frequency parameters.

2.6. Calibration

Both systems of pressure measurement were calibrated using the Pistomètre, a device developed by O.N.E.R.A. which provides a portable means of generating an oscillatory pressure at a required frequency. Before installing the model in the wind tunnel, calculated transfer functions of the pressure tubes were compared closely with laboratory measurements; agreement was good at the low levels of oscillatory pressure expected in the tests. The constants relating to each measuring channel were established before each wind-tunnel run; during the test the Pistomètre was used to provide a reference in one line of the pressure-switch systems.

3. Wind-Tunnel Tests

The tests were run in three phases, two covering low and moderate frequency parameters and the other covering high frequency parameters. Measurements were made at speeds of 12, 37, 55 and 73 m/sec at the frequencies available from the three sets of springs. Both part- and full-span control configurations were tested with control mean incidence settings of 0, $+3{\cdot}5$ and $-3{\cdot}5$ degrees; the amplitude of oscillation ranged from ± 2 to ± 5 degrees. A number of tests were also made with a transition strip attached near the leading edge. Some of the experimental results are listed in Tables 1 and 2, and illustrated in Figs. 6 to 24. Only a selection from the full record has been included in this report.

4. Theoretical Prediction of Loading Distribution

The loading distributions were obtained by application of lifting-surface theories. In lifting-surface theory the loading on the wing is approximated by a linear combination of a finite number of elementary functions of chordwise and spanwise variables which have the correct known behaviour of the loading at the edges of the wing. These elementary functions are chosen as the first few of a complete set. The coefficients are obtained by equating the upwash corresponding to the approximate loading to equivalent upwashes at a number of

upwash points on the wing surface. The upwash points form a network with m spanwise stations and n points on each spanwise station. If the loading has no singularities on the surface of the wing then the approximation to the loading can be good when m and n are small. The loading distribution corresponding to an oscillating control surface is singular around its inboard edges, the singularities having a logarithmic behaviour, and in consequence, higher values of m and n are required if the approximation to the loading is to give adequate accuracy.

Three theories were used for calculating the pressure distributions.

In the first approach the total lift, pitching moment and hinge moment have been calculated by a method of smooth, equivalent slopes continuing the principles of two-dimensional and slender-body theories in steady flow.[2,3] In this application the lifting-surface theory, and hence the final results, are only valid for low frequency-parameter conditions. Both full- and part-span control surfaces were treated; the results for lift and pitching moment have been checked by recourse to the reverse flow theorem.[3] For the full-span control, and with $n = 4$ the values of local lift, pitching moment and hinge moment have been used to construct the chordwise loading with the required logarithmic singularity in the real part and a weaker singularity in the imaginary part. A method has been applied (on the principles of the reverse-flow theorem) to give total lift and pitching moment at higher frequency parameters.

In the second theory the procedure used was that of taking more terms than has been customary in the loading distribution by means of a lifting-surface program developed by Long.[4] The number of terms that could be used was limited by the speed of the computer and the core capacity available. For a full-span control surface the singularity in the loading occurs mainly in the chordwise sense and this can be dealt with by taking high values of n. For example if $n = 16$, m had to be restricted to 4. The program of Long[4] is able to deal with this high value of n with good accuracy, whereas the accuracy of other less sophisticated programs tends to suffer when n becomes large. The value of m is unavoidably small, but the results for the full-span control are expected to converge quite rapidly with m when the aspect ratio is as low as 1·25. When a singular function is represented by a linear combination of a finite number of elementary functions, a feature of the resulting approximation is its undulatory behaviour. There are quite pronounced undulations in the results obtained for the real part of the loading for $n = 16$, $m = 4$. Despite this, the value of the approximate function is not far from the actual function except in the neighbourhood of the singularity where the infinite value of the real part of the loading at the leading edge of the control surface cannot be approached. However, this is not too serious for the total load, moment and hinge moment, all of which can be approximated quite well.

For a part-span control surface a high value of m would have to be used as well as a high value of n. It was not possible to calculate very satisfactory values for the part-span control configuration because of the relatively small number m of spanwise sections taken for the calculation. If for this wing planform m is taken to be > 10 then, because of the core size of the computer, n (the number of chordwise points) cannot be taken large enough to give a satisfactory estimate of the chordwise pressure distributions. The values used were (in the full-span case) $m = 4$, $n = 16$, and (in the part-span case) $m = 8$, $n = 12$.

In the third method an approximation to the loading was obtained from the work of Dat, Darovsky and Darras.[5,6] This approximation was modified by adding a function which was obtained from an imposed loading with the correct behaviour at the edges of the wing and the control surface. This additive function retained the singular behaviour at the junction between rigid oscillating surfaces; in particular the real part of the modified loading tended to infinity as the leading edge of the control surface was approached. The undulations mentioned earlier disappeared or were very much reduced in the modified loading function. Both full-span and part-span control surfaces were dealt with, though only a limited number of results was available for inclusion in this report.

Force coefficients obtained from theory are listed in Tables 1 and 2, and are illustrated in Fig. 6.

5. Discussion

Figs. 7 to 12 illustrate pressure distributions measured in the first phase of the tests at two values of frequency parameter along a number of chordwise sections on the upper surface of the model. Values have been interpolated where there was no pressure tapping on the chord in question. Tests were made in both full- and part-span configurations; the component loading coefficients plotted are

$$C'_p = \frac{\Delta p}{\frac{1}{2}\rho V^2} = \frac{2\bar{p}'}{\frac{1}{2}\rho V^2 \alpha} \qquad \text{(in-phase)}$$

and

$$C_p'' = \frac{\Delta p''}{\omega_R \cdot \frac{1}{2}\rho V^2} = \frac{2\bar{p}''}{v/2 \cdot \frac{1}{2}\rho V^2 \alpha} \qquad \text{(in-quadrature)}$$

where $\bar{p}$ is the perturbation pressure on one surface only
Δp is the perturbation loading
α is the amplitude of the oscillation (radians)
$'$ $''$ are superscripts denoting the in-phase and in-quadrature components.

The loading coefficients were defined in this form because the design of the model was such that it precluded simultaneous measurement of upper- and lower-surface pressures. Calculations of in-phase pressures, based on theory by Dat et al[5,6] appear to be somewhat greater than experiment. At the hinge line there is a logarithmic singularity which theory takes account of, and which was reflected by the pressure peak in the experimental results. Comparison of theoretical with experimental in-quadrature components was less satisfactory, especially in the region of the control; calculated values were half as large again as the corresponding experimental results. Some of the tests were repeated with a transition strip near the leading edge; its addition had only an insignificant effect on the results.

Measurements of oscillatory force coefficients were obtained in two ways—indirectly by integration of the measured pressure distribution and directly from strain-gauged balances. The results are listed in Tables 1 and 2, together with theoretical values.

A further series of tests was made at low and moderate values of v in the full-span control configuration using one pressure-switch system only. Pressure distributions have been calculated using the theories of Garner[2,3] and Long;[4] for the purpose of comparison the undulations resulting from calculations by Long's method have been faired by a smooth curve (Figs. 13 to 17).

Fig. 13 illustrates in-phase and in-quadrature upper- and lower-surface pressure components at a section $\eta = 0{\cdot}68$ at 73 m/sec and $v = 0{\cdot}88$. At this frequency parameter the two sets of calculation gave very similar results. Both predicted in-phase pressure distributions with adequate accuracy, and both over-estimated the in-quadrature values.

Figs. 14 and 15 illustrate upper- and lower-surface pressures at section $\eta = 0{\cdot}68$ and $\eta = 0{\cdot}92$, at a wind speed of 37 m/sec and $v = 3{\cdot}40$. At both sections calculations of in-phase components, based on Long's theory, agreed well with experiment over the final part of the wing: quantitative agreement over the control was rather poor. Theory over-estimated in-quadrature components over wing and control.

Figs. 16 and 17 show pressure distributions at $\eta = 0{\cdot}68$ for the same wind-tunnel conditions but with the control set to mean deflections of $\beta = -3{\cdot}5$ and $+3{\cdot}5$ degrees. Pressure distributions overall were broadly similar to those measured in the $\beta = 0$ degrees test (Fig. 15) and the earlier comments made about the comparison between theory and experiment also apply to these results.

One rather disappointing feature of these tests was the disparity between pressures on upper and lower surfaces; when the control was deflected to $\beta = -3{\cdot}5$ degrees the disparity occurred over the fixed portion of the wing, and when $\beta = +3{\cdot}5$ degrees it occurred over the control.

The final phase of testing was carried out at high values of v. Fig. 18 shows in-phase and in-quadrature pressures measured at an inboard section in the full-span control configuration. Pressures measured on the port wing compared well with pressures measured at the corresponding station on the starboard wing. However, the disparity over the control surface between in-phase pressures measured on the upper surface and those measured on the lower surface is large—considerably more marked than the similar disparity noted at lower frequency parameter. The in-quadrature pressure distributions appear to be substantially the same on both surfaces of both port and starboard wings. There is some scatter in the measured values. Fig. 19 illustrates pressures measured in the same tests at a mid-span station.

Pressure distributions in the part-span configuration are illustrated in Figs. 20 to 24. Measurements were made over the lower surface of the port wing and the upper surface of the starboard wing. The in-phase pressure distributions are very similar over the fixed portion of the wing but differ widely over the control surface; for example (Fig. 20 (a)) the difference in pressure coefficients at an inboard section is of the order of 4. Characteristics are very similar at sections near the mid-span. The unsteady pressures decrease rapidly over the fixed portion of the wing outboard of the control. The in-quadrature pressure distributions do not differ significantly from those measured in the full-span configuration. Scatter of the experimental values appears to be small.

Experimentally measured force coefficients (Tables 1 and 2) were generally lower than calculated values; in general they followed the same trends as the oscillatory pressure distributions.

All the pressure measurements showed some degree of scatter though results obtained from the pressure-switch system were markedly more consistent than those obtained from the individual transducers. This was an important advantage in an experiment of this kind where the oscillatory pressures to be measured were very small. One drawback of both installations was an inability to record upper and lower surface pressures simultaneously.

It is difficult to draw any firm conclusions from a comparison of theory and experiment because of the very large differences between the in-phase measurements on upper and lower surfaces at the higher frequency parameters. The most that can be said is that theoretical and experimental pressure distributions are broadly similar in pattern. A quantitative comparison over the whole range is inconclusive. Averaged in-phase pressure measurements over upper and lower surfaces vary between about three-quarters and one-half of the corresponding calculated values, and a similar result is obtained by averaging in-quadrature measurements over upper and lower surfaces and comparing these mean pressures with the equivalent theoretical values.

The major differences between theory and experiment occur over the surfaces of the control. When disparities were first noted at the lower frequency parameters, some effort was made to discover if these were caused by irregularities in the flow of the tunnel or by the geometry of the model and mounting. Static tests showed that the pressure distributions on upper and lower surfaces were symmetrical about the median plane. In oscillatory tests, however, it was observed that small disparities existed even at zero wind speed. Time did not permit a full investigation of this problem; it is very possible, however, that the differences arose because of the asymmetric location of the sealing membrane between wing and control surface with respect to the median plane through the wing. The seal was attached to the inside surface of one skin each of the wing and the control. The interior of the model (which was hollow) was thus vented to one surface of the wing rather than the other.

6. Concluding Remarks

This experiment has shown that unsteady pressures and oscillatory forces on a wing with an oscillating control surface can be measured in low-speed flow over quite wide ranges of frequency parameter. Calculations were made using theories developed by Garner et al, Long and Dat et al; the theories gave results which were in reasonable agreement with each other. The sets of experimental results were consistent in themselves. A comparison of calculated in-phase pressure distributions over the fixed portion of the wing with measurements showed that calculation followed the experimental trends but predicted higher oscillatory pressure levels; at higher frequency parameters the in-phase pressures measured on the upper surface of the control differed markedly from those measured on the lower surface. All the in-quadrature pressure distributions were overestimated. Thus no firm conclusions could be drawn from a comparison of theory and experiment. Similar comments apply to the comparison of calculated and measured oscillatory forces.

Small mean deflections of the control surface did not significantly affect the oscillatory pressure distribution, nor was there any marked effect when a transition strip was added.

The tests provided an opportunity for comparing two pressure measuring installations, one based on individual transducers, the other on multiple pressure tappings connected to a single transducer via a pressure switch. Test results from the pressure switch system were altogether more consistent than the results from the individual transducers—a considerable advantage when the oscillatory pressure level is very low.

Acknowledgements

The author wishes to thank the many members of O.N.E.R.A. and R.A.E. who helped at every stage of this programme.

LIST OF SYMBOLS

$2b = c$	Wing chord
C'_p	$\frac{\Delta p'}{\frac{1}{2}\rho V^2}$
C''_p	$\frac{\Delta p''}{\frac{1}{2}\rho V^2}$
$C''_{p}{}'$	$\frac{2C''_p}{\nu}$
m	Number of spanwise sections on wing taken as the basis for the R.A.E. and N.P.L. calculations
n	Number of chordwise points on each spanwise section
$\bar{p}$	Perturbation pressure locally on one surface
V	Wind speed (m/s)
x	Chordwise co-ordinate
α	Amplitude of control oscillation wind on, (radians)
β	Mean deflection of control (degrees) (+ ve nose up)
Δp	$\frac{\bar{p}}{\alpha}$
η	Non-dimensional spanwise co-ordinate
ρ	Air density
ω	Angular frequency
ν	Frequency parameter $\frac{2\omega b}{V}$
$'$	Superscript denoting in-phase component
$''$	Superscript denoting in-quadrature component

REFERENCES

No.	*Author(s)*	*Title, etc.*
1	H. Bergh and H. Tidjeman ..	Theoretical and experimental results for the dynamic response of pressure measuring systems. N.L.R. TR-F 238 (1965).
2	H. C. Garner and Doris E. Lehrian	The theoretical treatment of slowly oscillating part-span control surfaces in subsonic flow. A.R.C. R. & M. 3676 (1969).
3	Doris E. Lehrian and H. C. Garner	Comparative numerical applications of the reverse flow theorem to oscillating wings and control surfaces. A.R.C. R. & M. 3488 (1965).
4	G. Long	An improved method for calculating generalised air forces on oscillating wings in subsonic flow. A.R.C. R. & M. 3657 (1969).
5	R. Dat, L. Darovsky and B. Darras	Considerations sur la solution matricielle du problème portant instationnaire en subsonique, et application aux gouvernes. O.N.E.R.A. Note Technique 135 (1968).
6	R. Dat and B. Darras	Calcul du champ de pression induit par l'oscillation d'une gouverne en écoulement subsonique. Paper presented at the 29th meeting of A.G.A.R.D. Structures Panel (1969).
7	W. D. T. Hicks	A control and measurement system for aeroelastic model tests. A.R.C. C.P. 1045 (1968).

TABLE 1

Force Coefficients (Full-Span Control Surface)

			$v =$	0	0·88	1·0	1·50	2·70	3·0	3·4	6·0	6·6	7·04	8·0
k'_d	Theory	Garner		1·406			1·267		0·966*		−0·18*			
		Dat		1·40		1·30		1·08						
		Long			1·369		1·293		0·943	0·829		−0·510	−0·762	−1·341
	Experiment	Pressures				0·935		0·730						
		Direct				0·950		0·730						
k''_d	Theory	Garner		2·10 v			0·876		1·795*		3·68*			
		Dat		2·30 v		0·575		1·58						
		Long			0·461		0·839		1·742	1·958		3·980	4·238	4·880
	Experiment	Pressures				0·320		0·865						
		Direct				0·400		0·980						
m'_d	Theory	Garner		0·127			0·110		−0·017*		−0·600*			
		Dat		0·126		0·126		0·0285						
		Long			0·143		0·119		−0·027	−0·075		−0·702	−0·810	−1·089
	Experiment	Pressures				0·0542		0·0156						
		Direct				0·064		0·019						

m''_d	Theory	Garner	1·14 v			0·369		0·713*		1·39*			
		Dat	1·008 v		0·232		0·564						
		Long		0·207		0·363		0·684	0·762		1·512	1·606	1·840
	Experiment	Pressures			0·0731		0·196						
		Direct			0·0780		0·210						
n'_d	Theory	Garner	0·103										
		Dat			0·090		0·0219		−0·020				−0·512
		Long		0·103		0·083		−0·018	−0·029		−0·376	−0·426	−0·572
	Experiment	Pressures			0·070		0·0249						
		Direct			0·081								
n''_d	Theory	Garner	0·48 v										
		Dat	0·46 v		0·115		0·320	0·400	0·470				0·98
		Long		0·093		0·168		0·340	0·380		0·778	0·844	0·954
	Experiment	Pressures			0·071		0·192						
		Direct			0·080		0·216						

* The last place in these values is only accurate to within ±3.

TABLE 2

Force Coefficients (Part-Span Control Surface)

v			0	1·00	1·50	2·70	3·00	6·00
k'_d	Theory	Garner	0·992		0·896		0·687*	−0·11*
		Dat	0·995	0·945		0·765		
	Experiment	Pressures		0·606		0·472		
		Direct		0·661		0·580		
k''_d	Theory	Garner	1·44 v		0·608		1·248*	2·56*
		Dat	1·60 v	0·398		1·10		
	Experiment	Pressures		0·216		0·582		
		Direct		0·300		0·800		
m'_d	Theory	Garner	0·080		0·070		−0·015*	−0·41*
		Dat	0·078	0·080		0·0166		
	Experiment	Pressures		0·0415		0·057		
		Direct		0·0138		0·011		
m''_d	Theory	Garner	0·78 v		0·248		0·479*	0·93*
		Dat	0·68 v	0·017		0·419		
	Experiment	Pressures		0·0378		0·094		
		Direct		0·0350		0·100		
n'_d	Theory	Garner	0·059					
		Dat	0·0575	0·050		0·0215		
	Experiment	Pressures		0·041		0·0159		
		Direct		0·050				
n''_d	Theory	Garner	0·28 v	0·070				
		Dat	0·276 v	0·069		0·187		
	Experiment	Pressures		0·0361		0·0975		
		Direct		0·051		0·136		

* The last place in these values is only accurate to within ± 3.

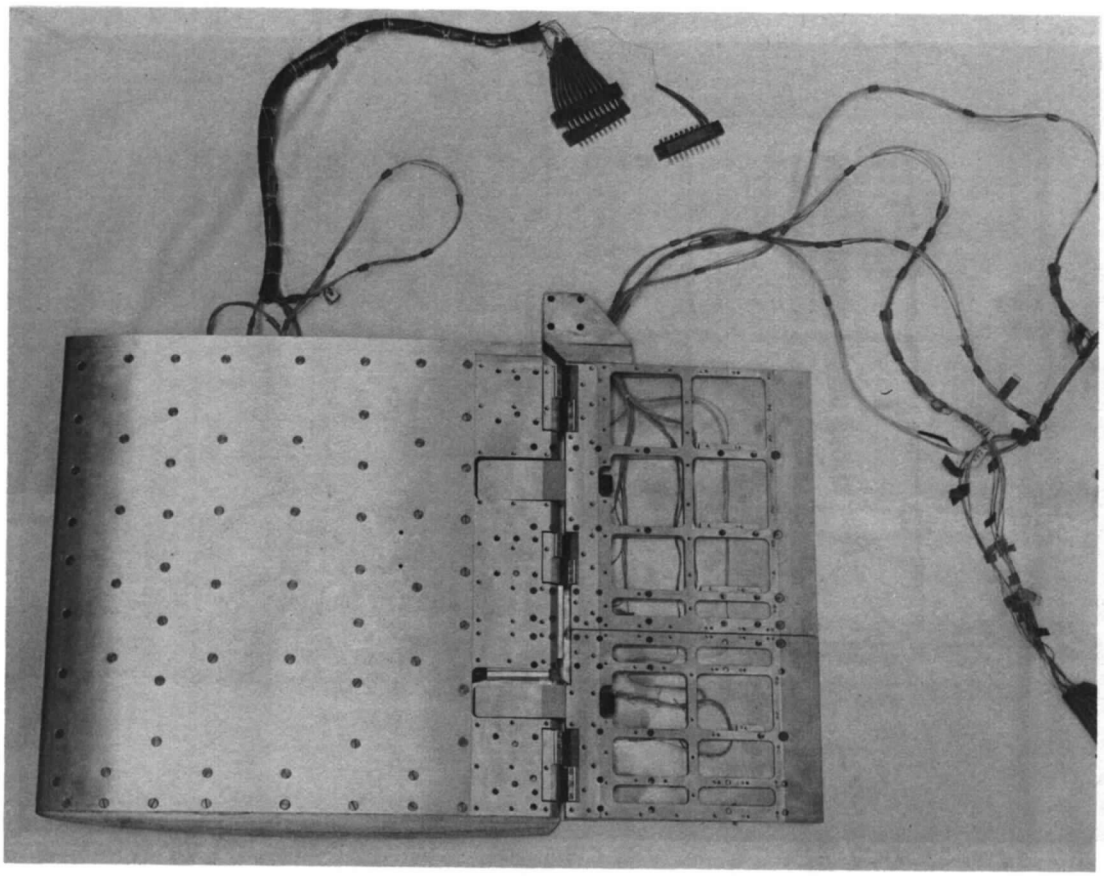

FIG. 1. Starboard under side, installation of individual transducers.

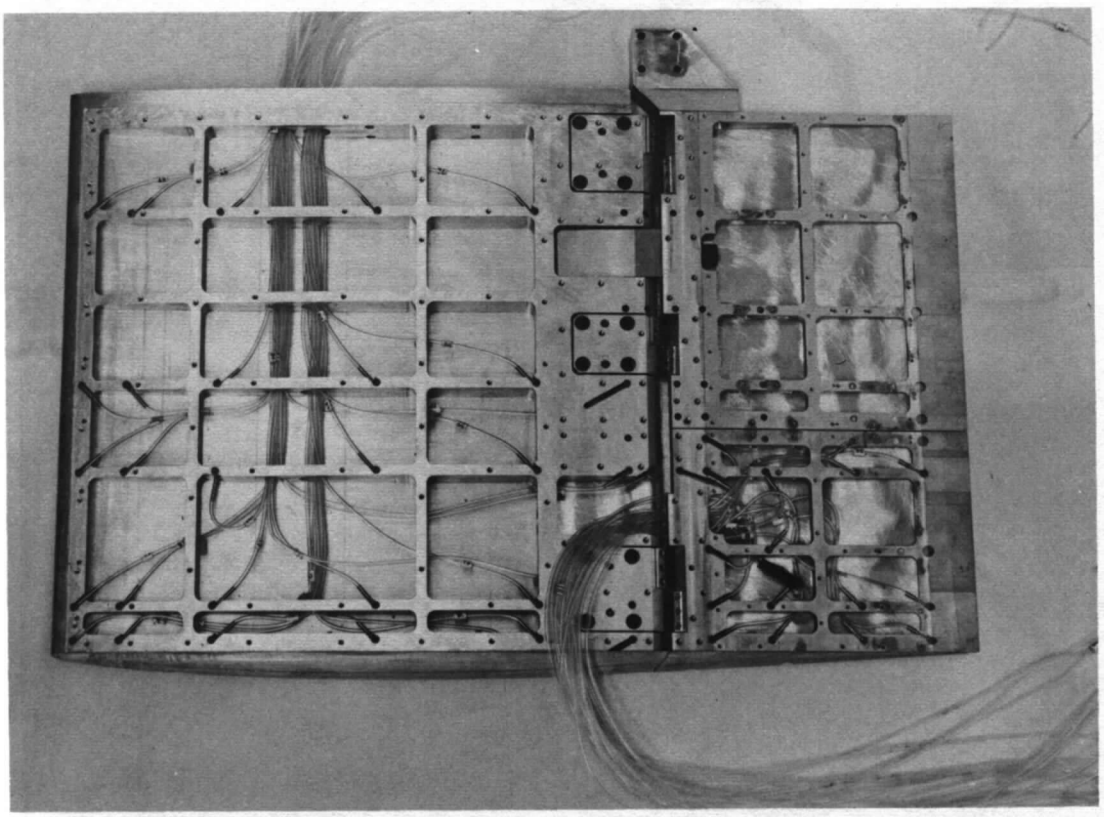

FIG. 2. Port upper side, installation of tubed pressure measuring system.

FIG. 3. Calibration of model.

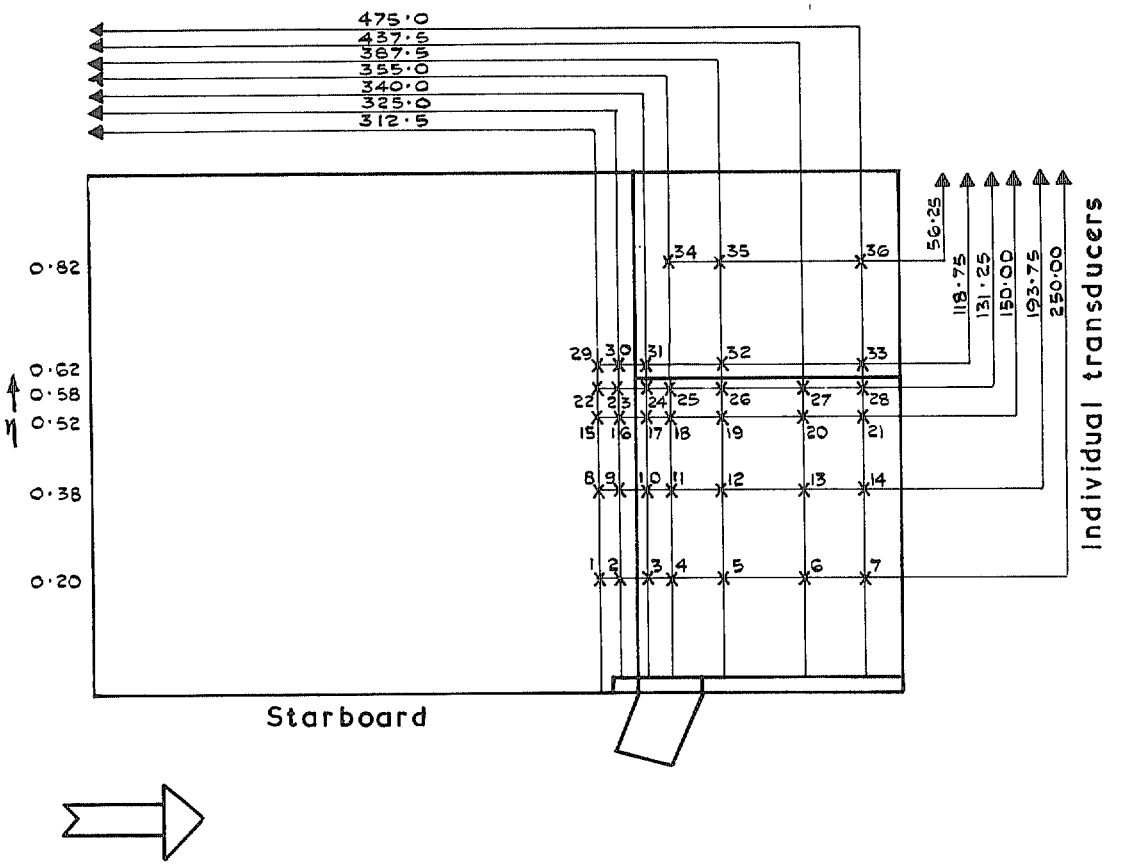

Positions of individual pressure transducers

FIG. 4. Pressure measuring stations (dim/in/mm).

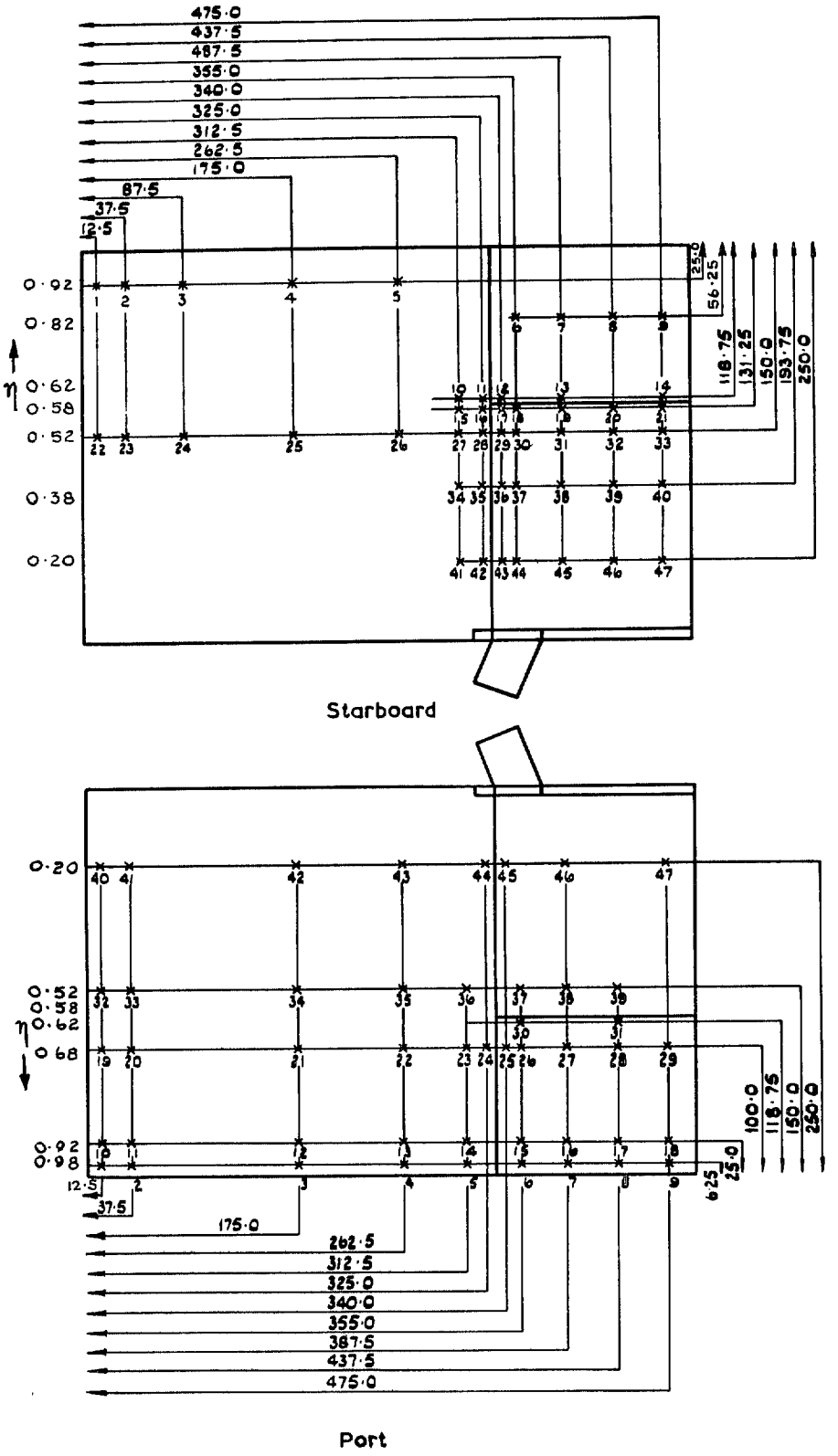

Scani valve systems and position of pressure tappings

FIG. 4 continued.

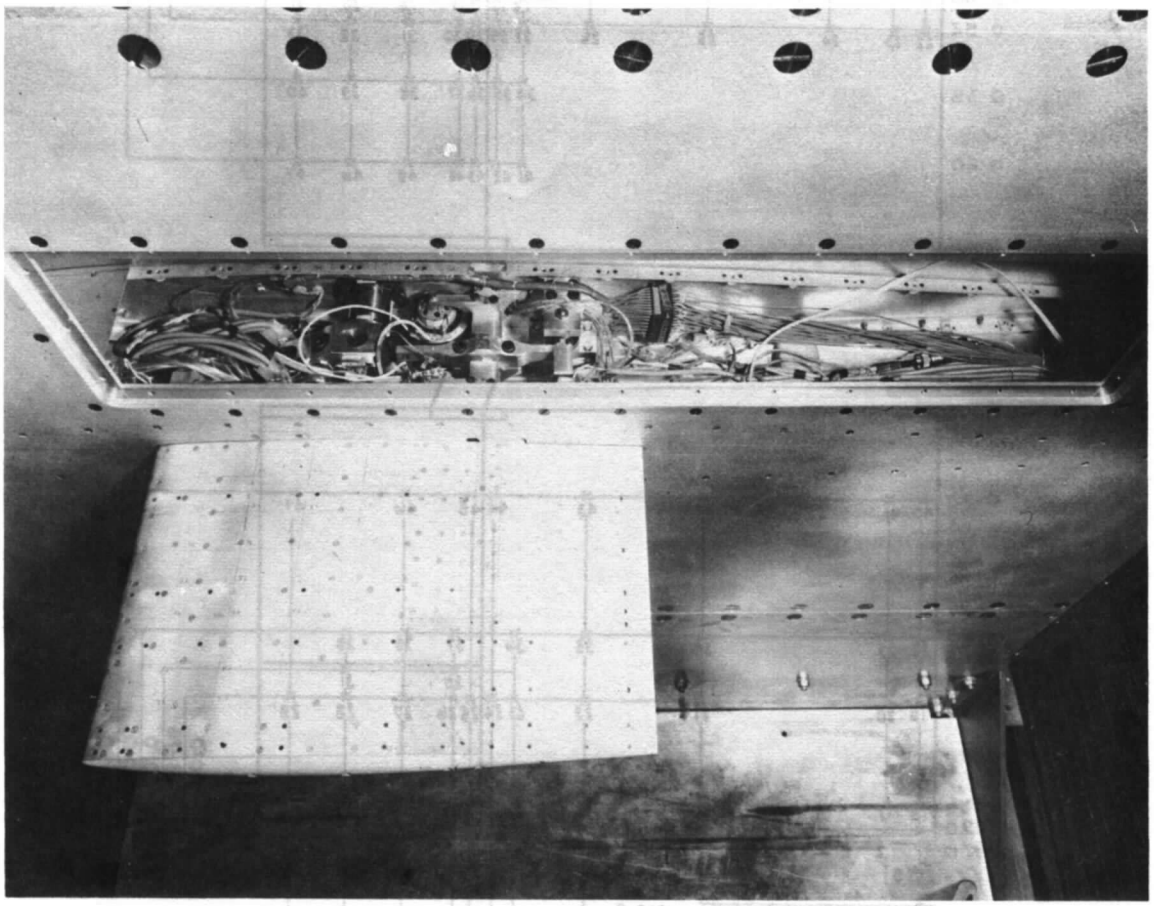

FIG. 5. Interior of nacelle, showing excitation system and Scanivalve.

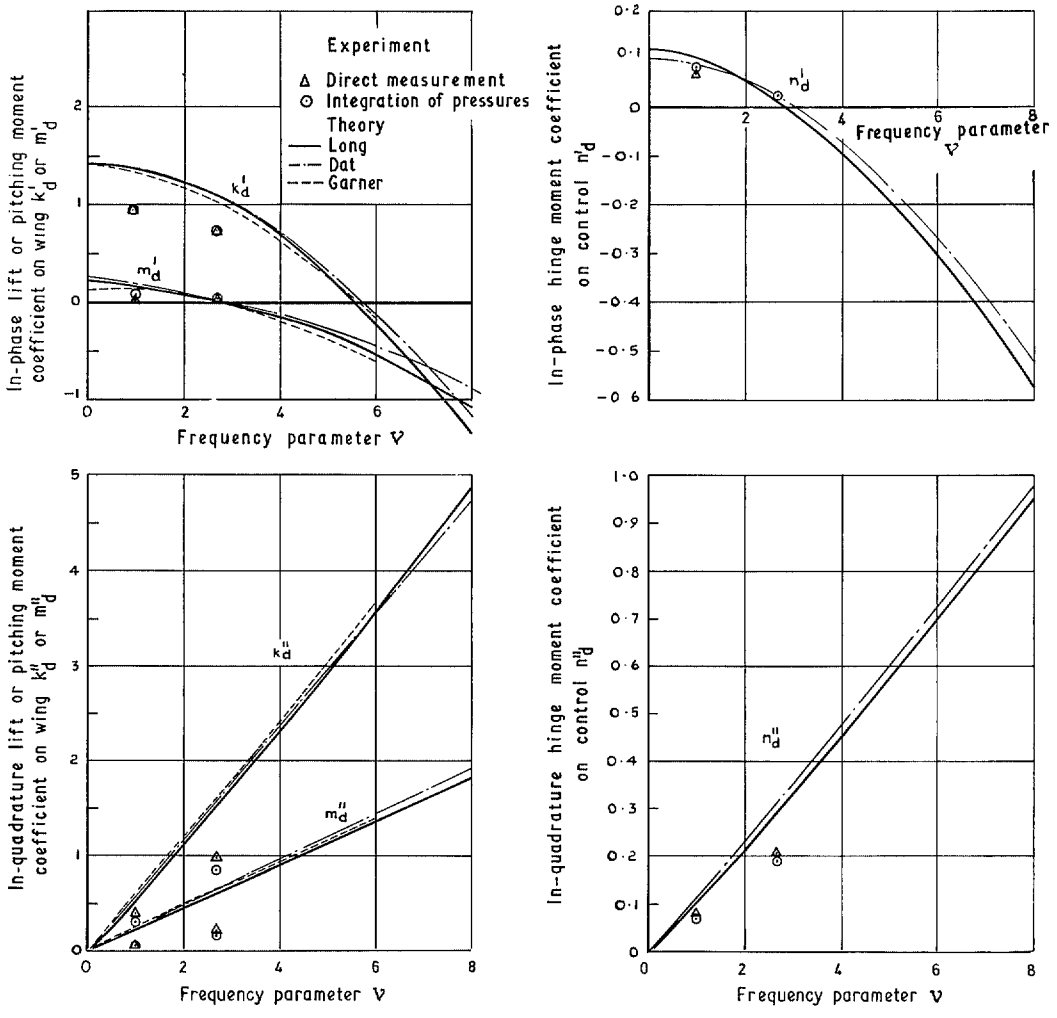

FIG. 6. Force coefficients (full-span control surface).

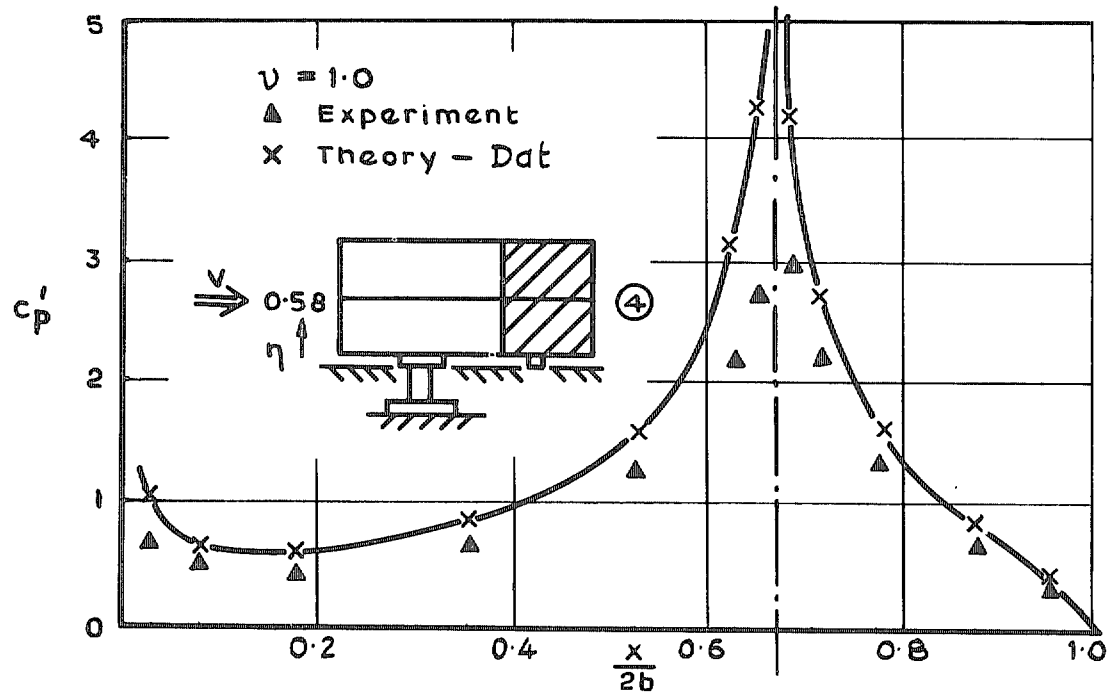

(a) In-phase loading coefficient

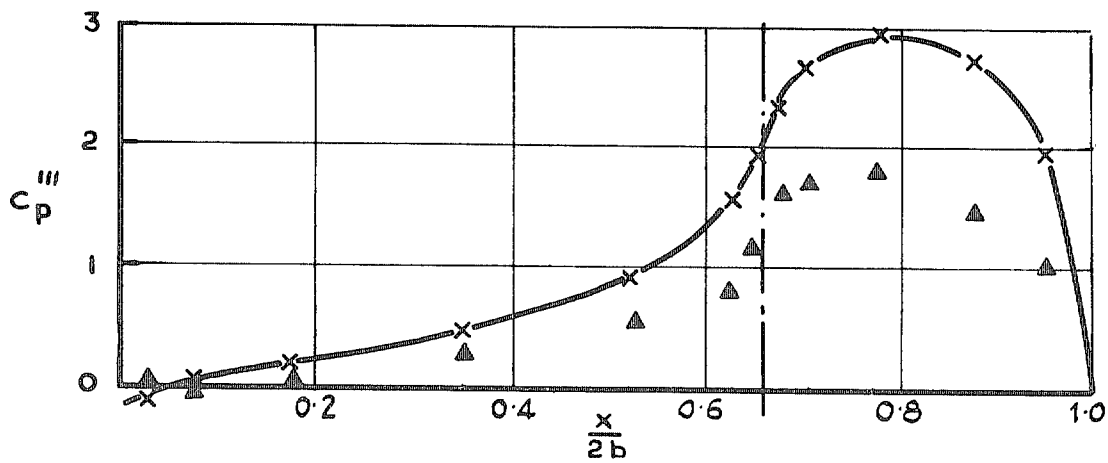

(b) In-quadrature loading coefficient

FIG. 7 (a) and (b). Loading coefficients at $\eta = 0{\cdot}58$—full-span control.

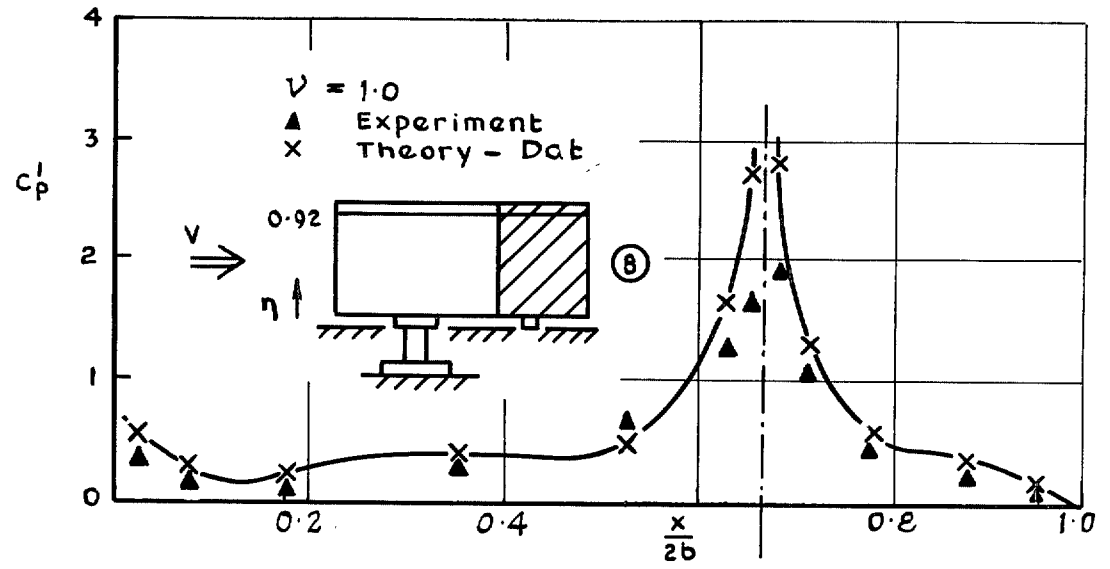

(a) In-phase loading coefficient

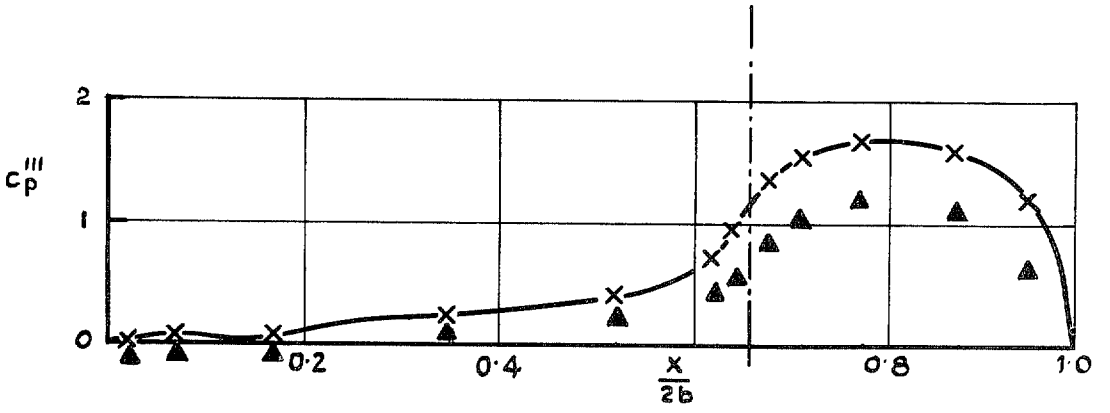

(b) In-quadrature loading coefficient

FIG. 8 (a) and (b). Loading coefficients at $\eta = 0{\cdot}92$—full-span control.

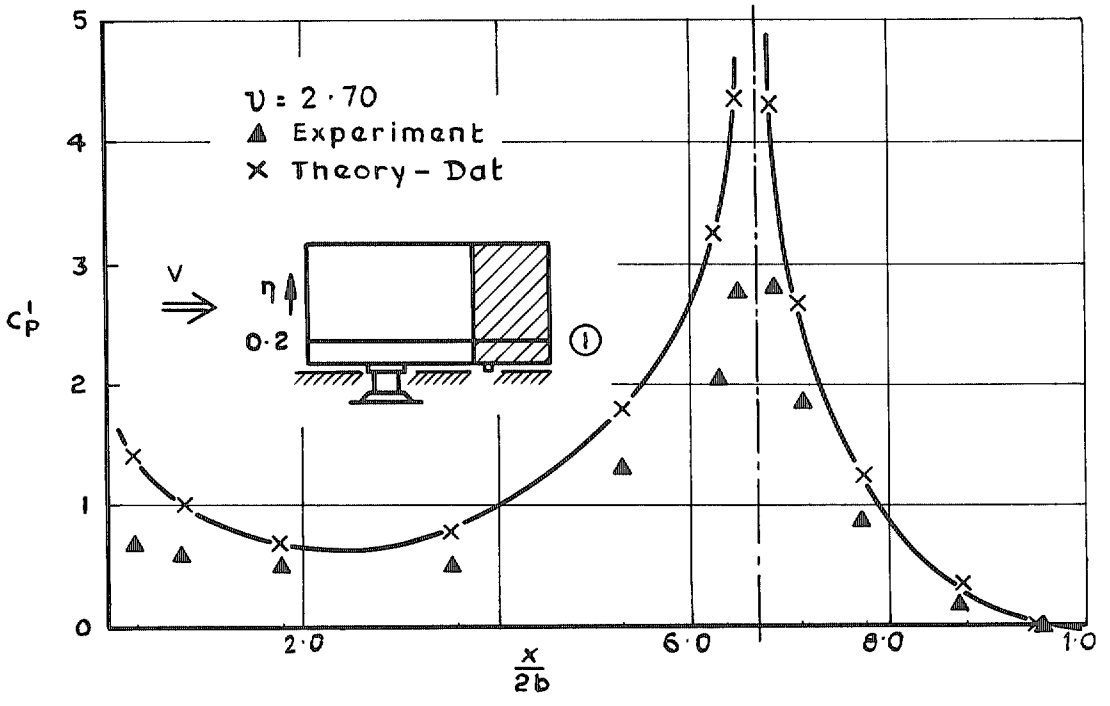

(a) In-phase loading coefficient

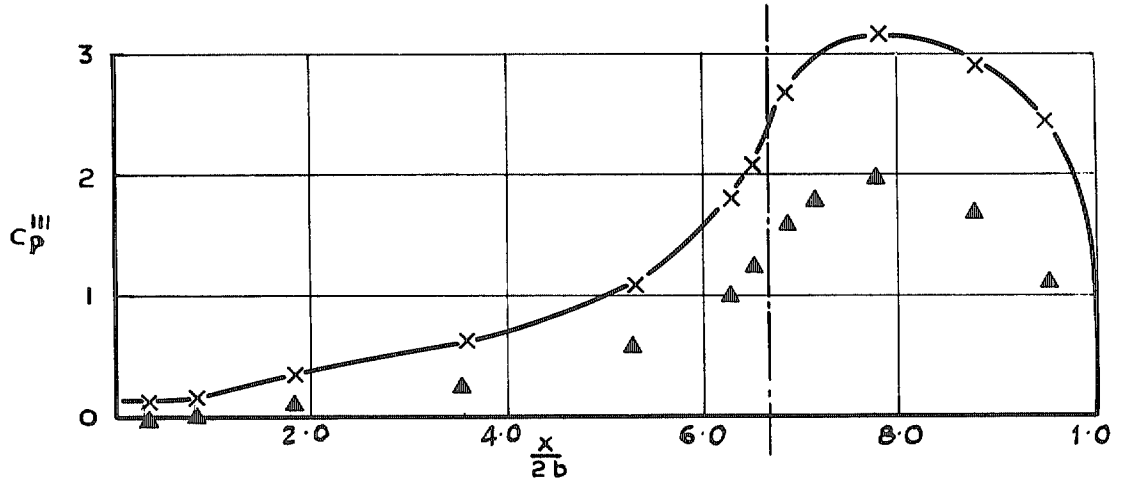

(b) In-quadrature loading coefficient

FIG. 9 (a) and (b). Loading coefficients at $\eta = 0{\cdot}2$—full-span control.

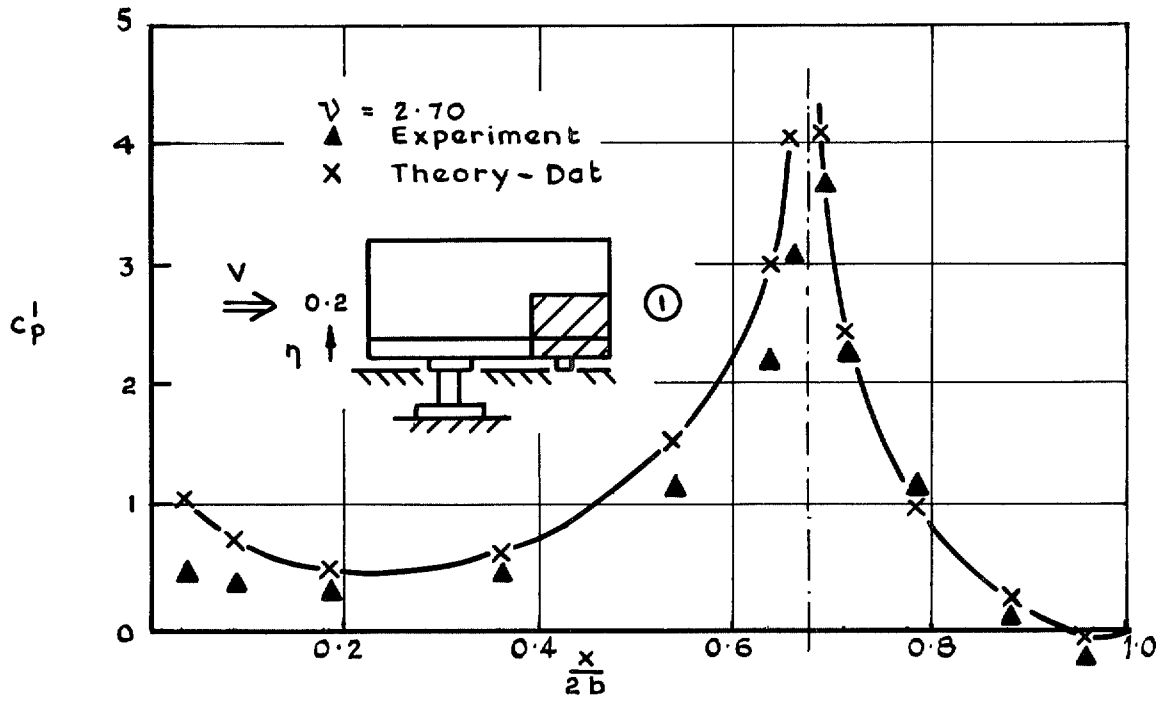

(a) In-phase loading coefficient

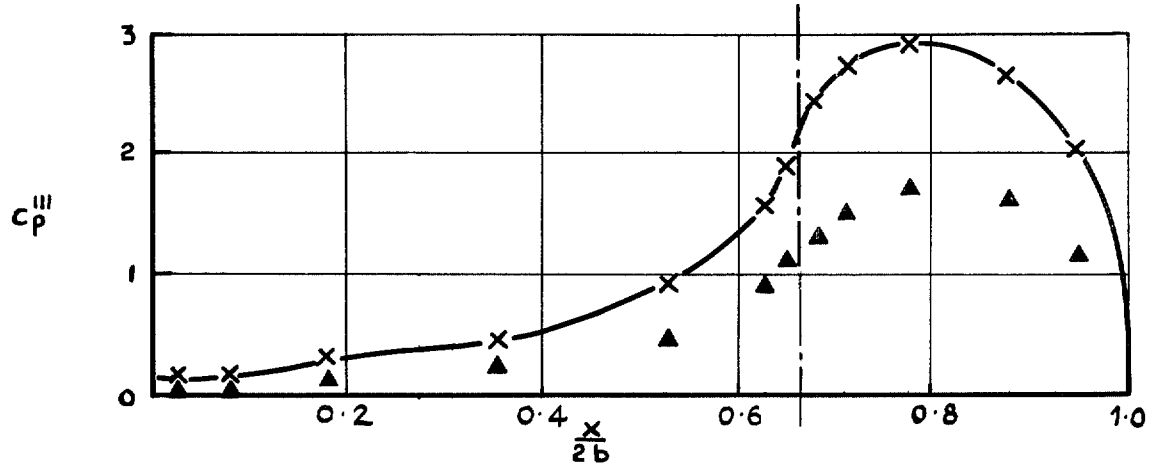

(b) In-quadrature loading coefficient

FIG. 10 (a) and (b). Loading coefficients at $\eta = 0.2$—part-span control.

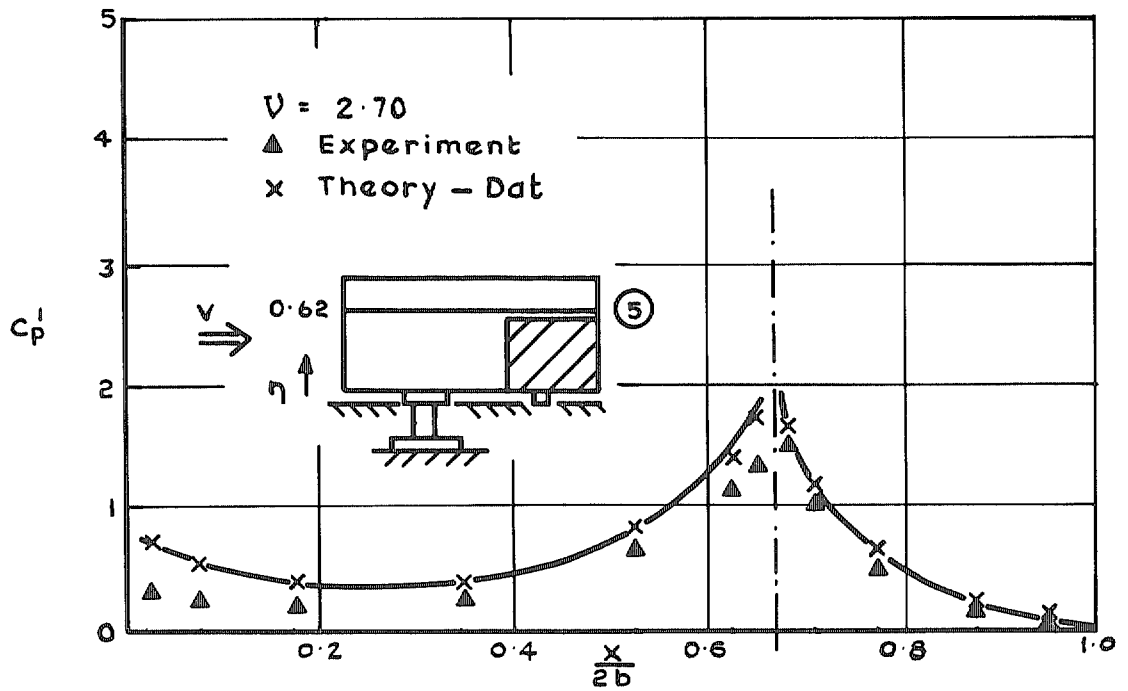

(a) In-phase loading coefficient

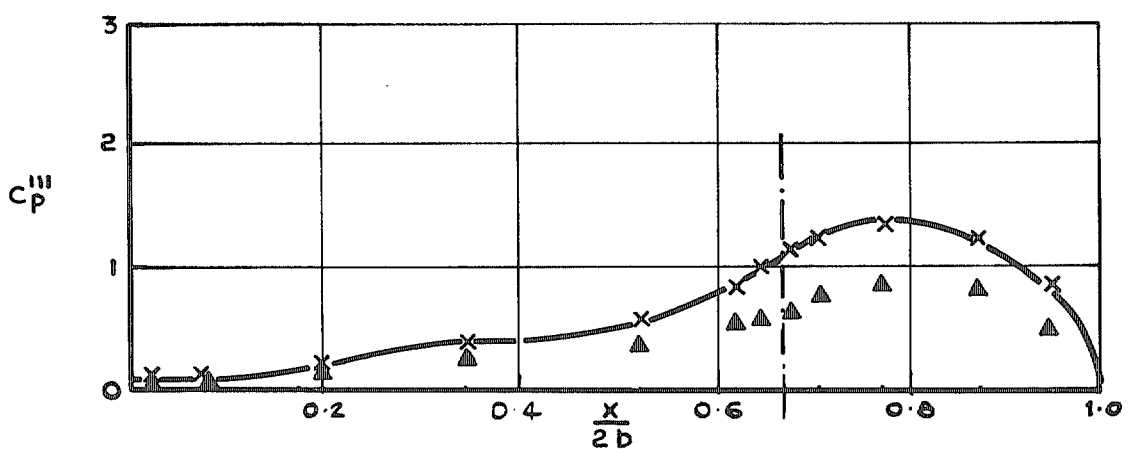

(b) In-quadrature loading coefficient

FIG. 11 (a) and (b). Loading coefficients at $\eta = 0{\cdot}62$—part-span control.

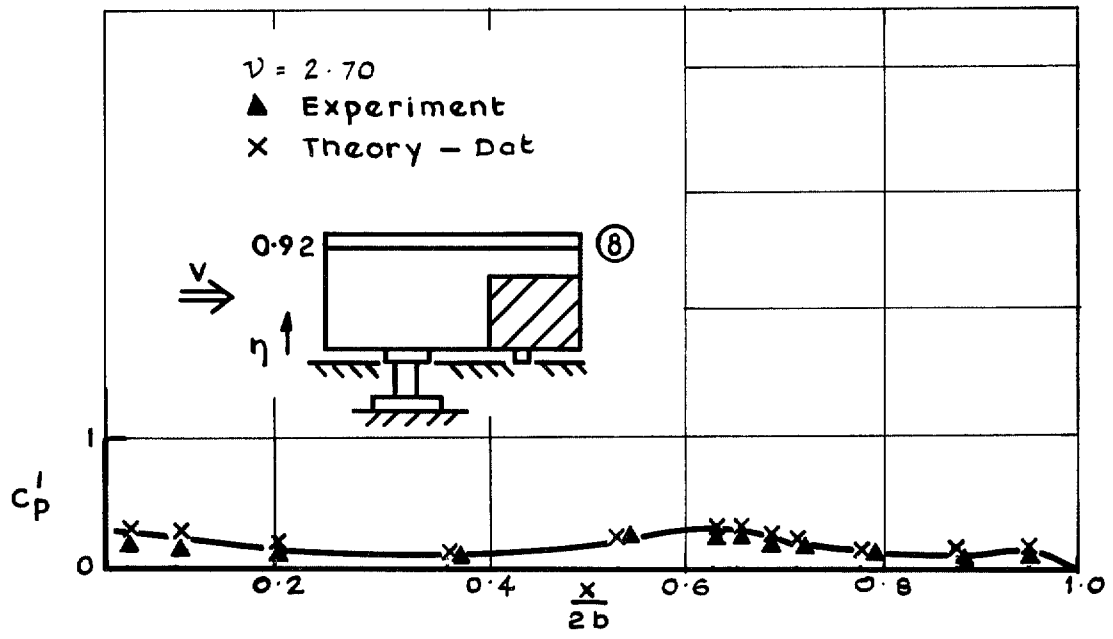

(a) In-phase loading coefficient

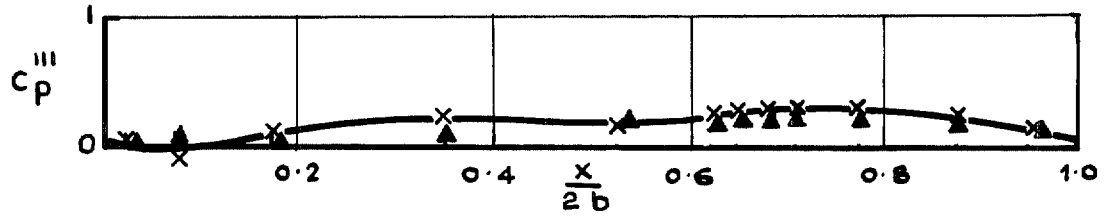

(b) In-quadrature loading coefficient

FIG. 12 (a) and (b). Loading coefficients at $\eta = 0{\cdot}92$—part-span control.

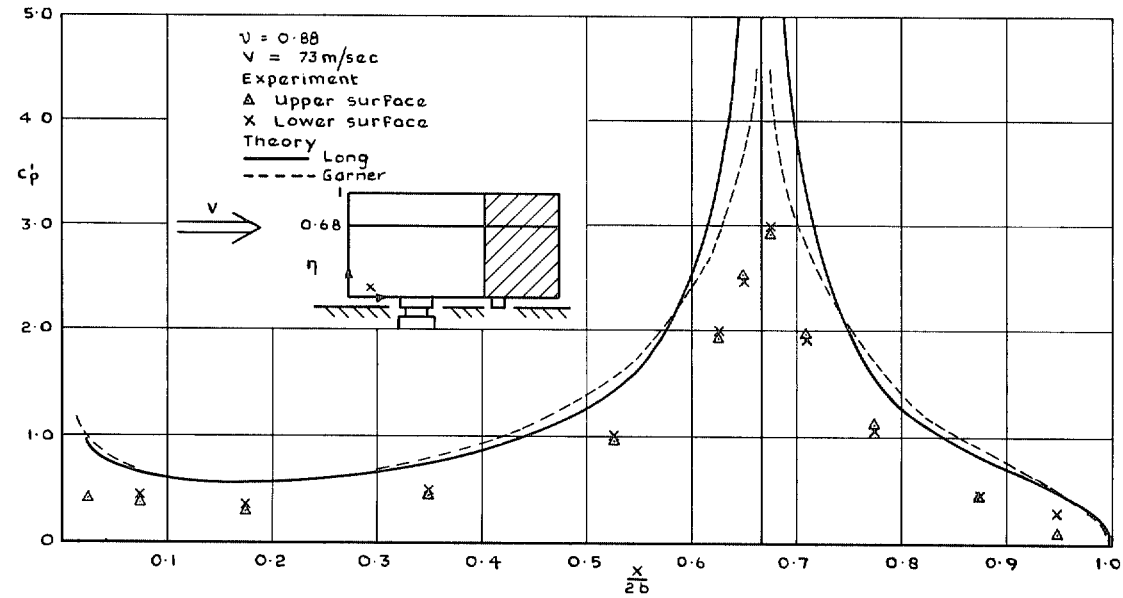

(a) In-phase loading coefficient

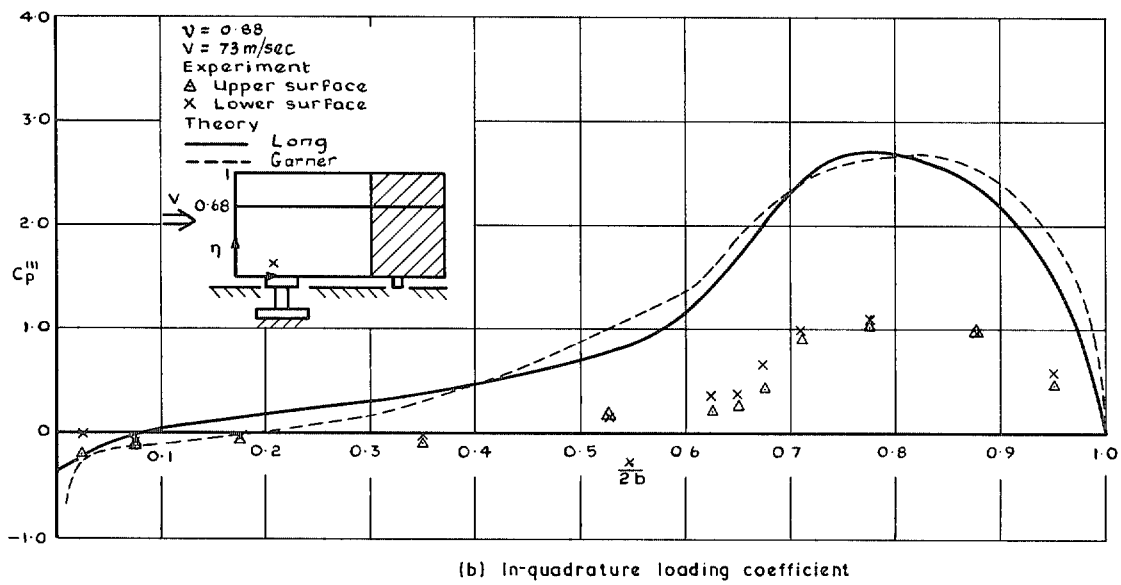

(b) In-quadrature loading coefficient

FIG. 13 (a) and (b). Loading coefficients at $\eta = 0{\cdot}68$—full-span control.

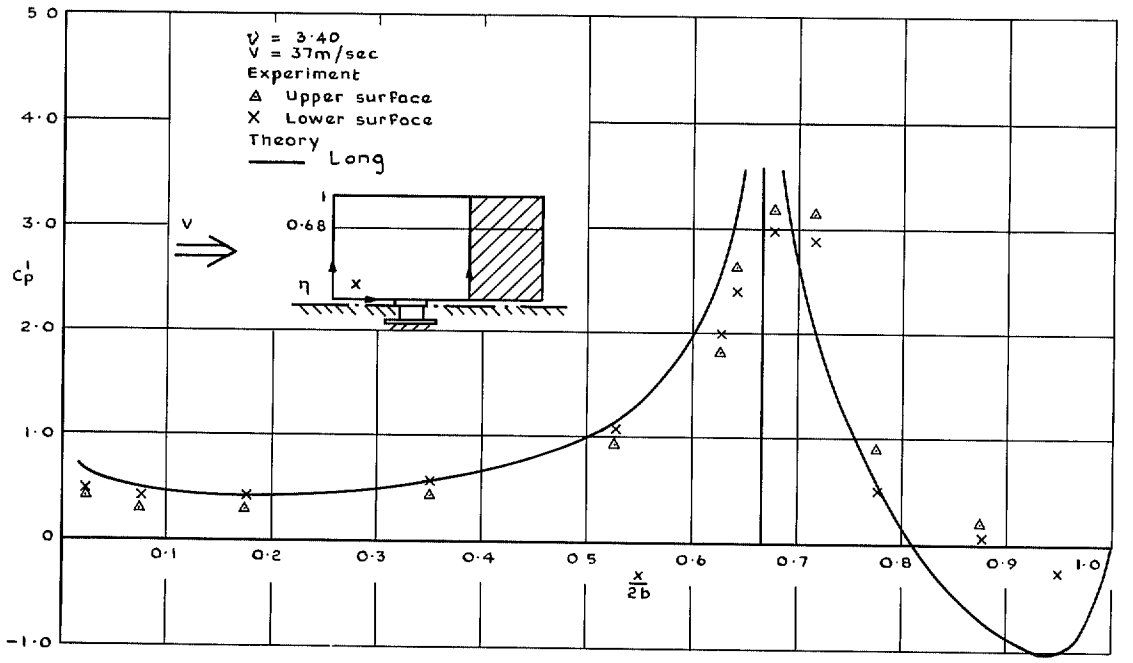

(a) In-phase loading coefficient

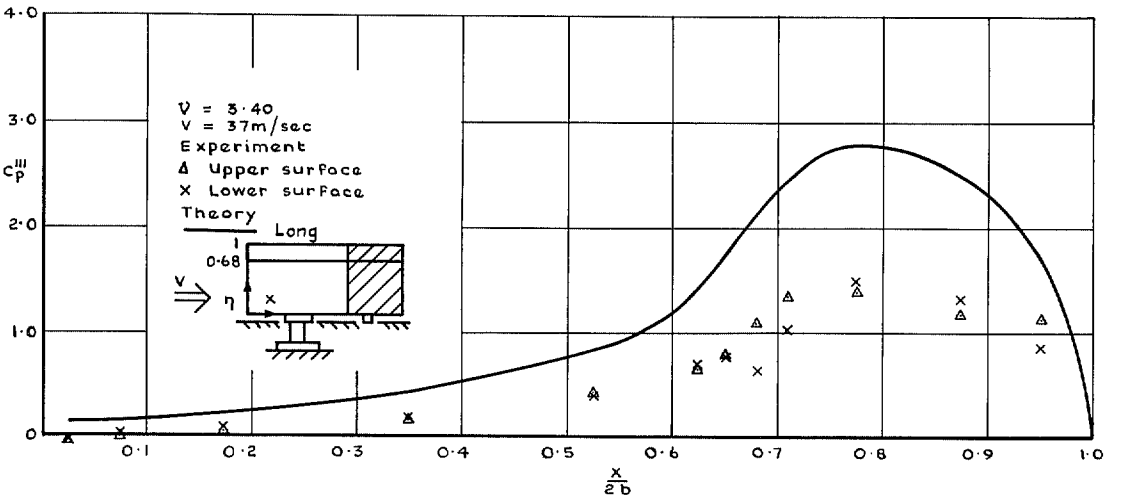

(b) In-quadrature loading coefficient

FIG. 14 (a) and (b). Loading coefficients at $\eta = 0{\cdot}68$—full-span control.

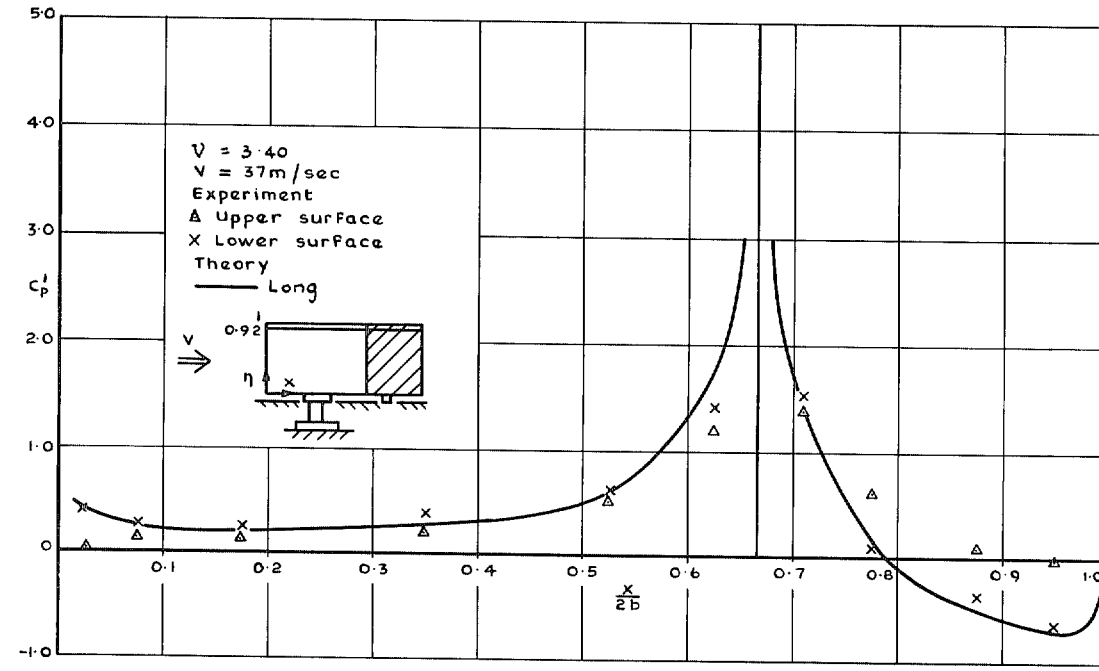

(a) In-phase loading coefficient

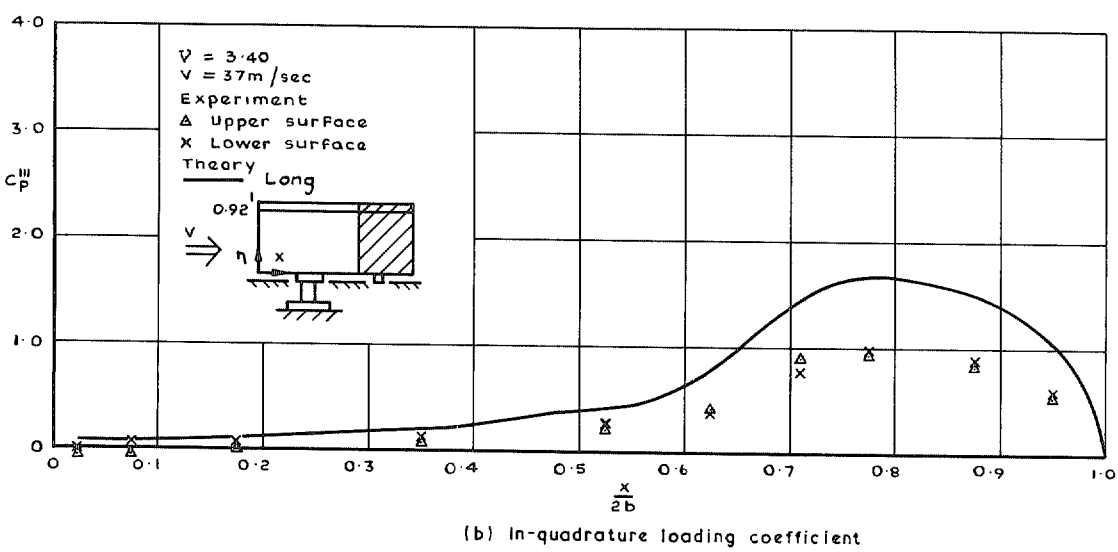

(b) In-quadrature loading coefficient

FIG. 15 (a) and (b). Loading coefficients at $\eta = 0{\cdot}92$—full-span control.

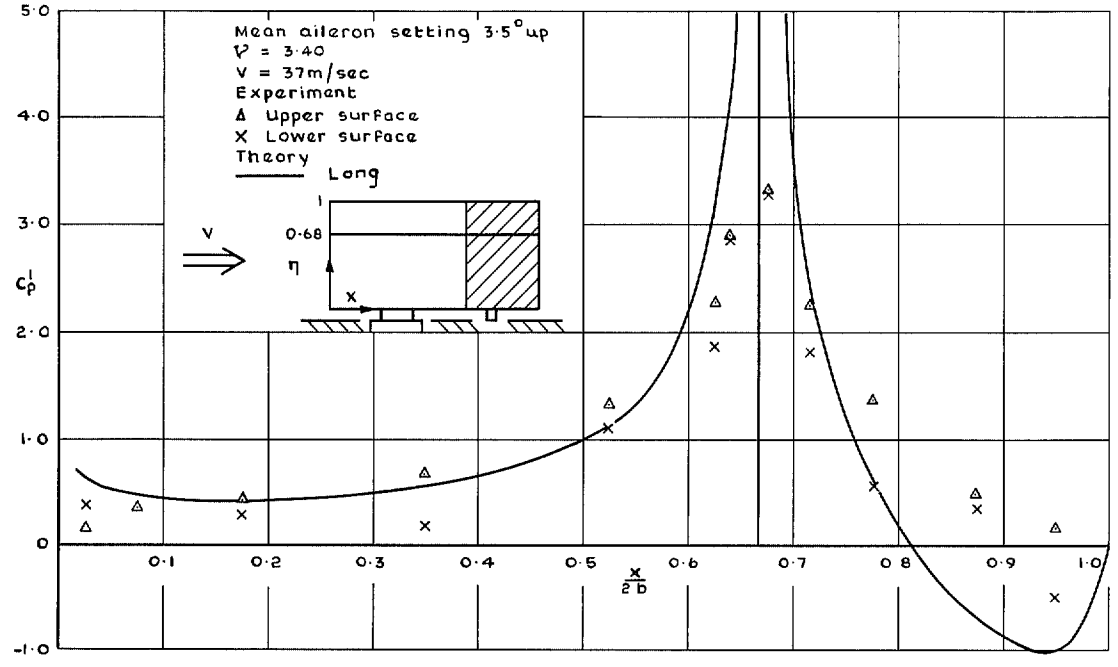

(a) In-phase loading coefficient

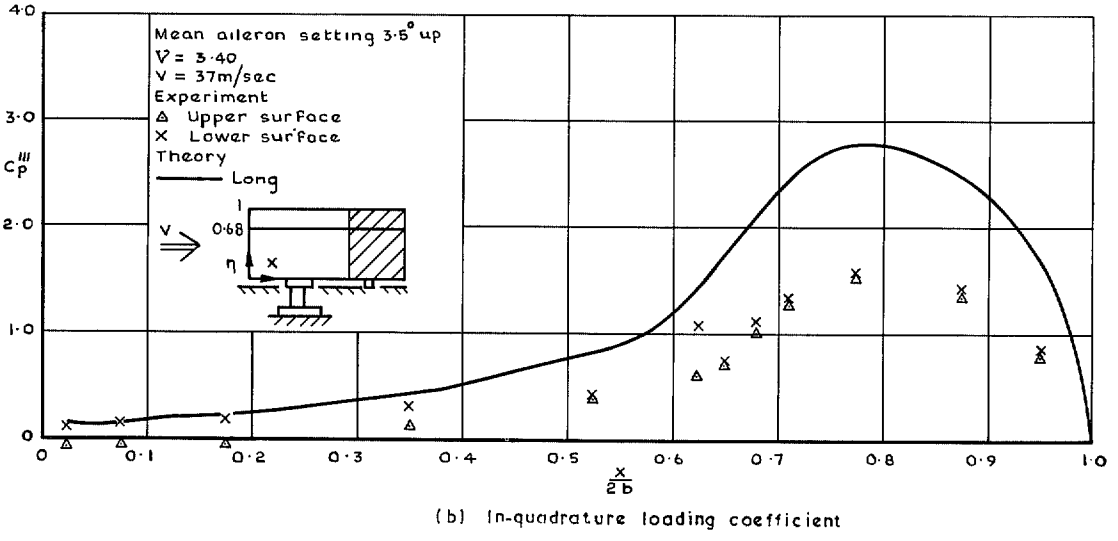

(b) In-quadrature loading coefficient

FIG. 16 (a) and (b). Loading coefficients at $\eta = 0{\cdot}68$—full-span control.

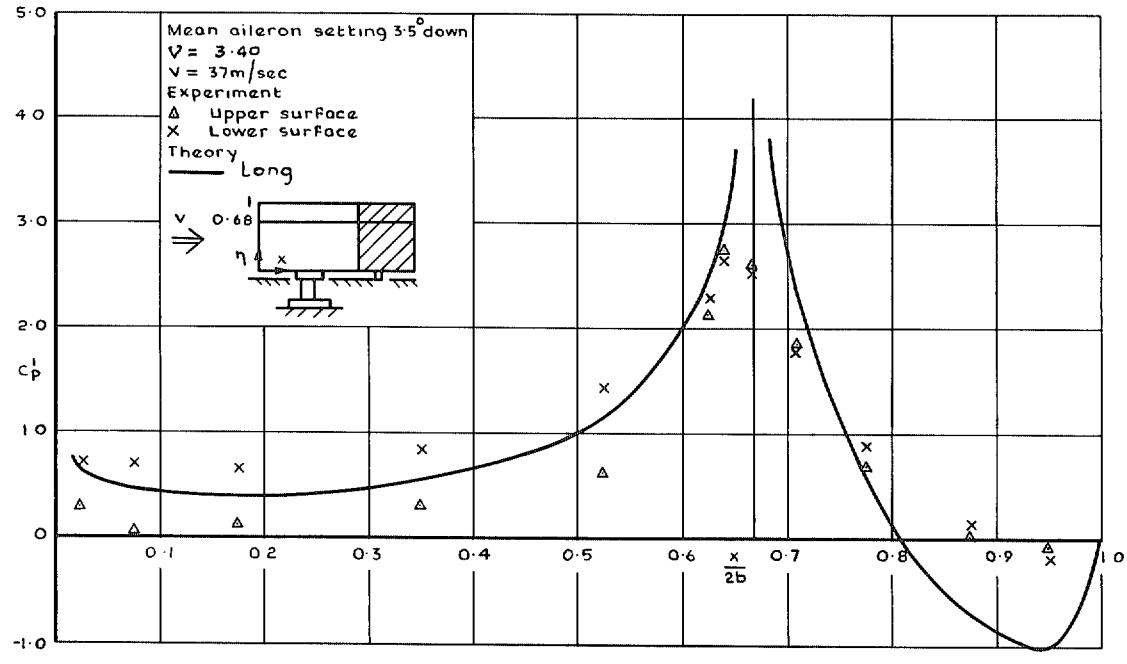

(a) In-phase loading coefficient

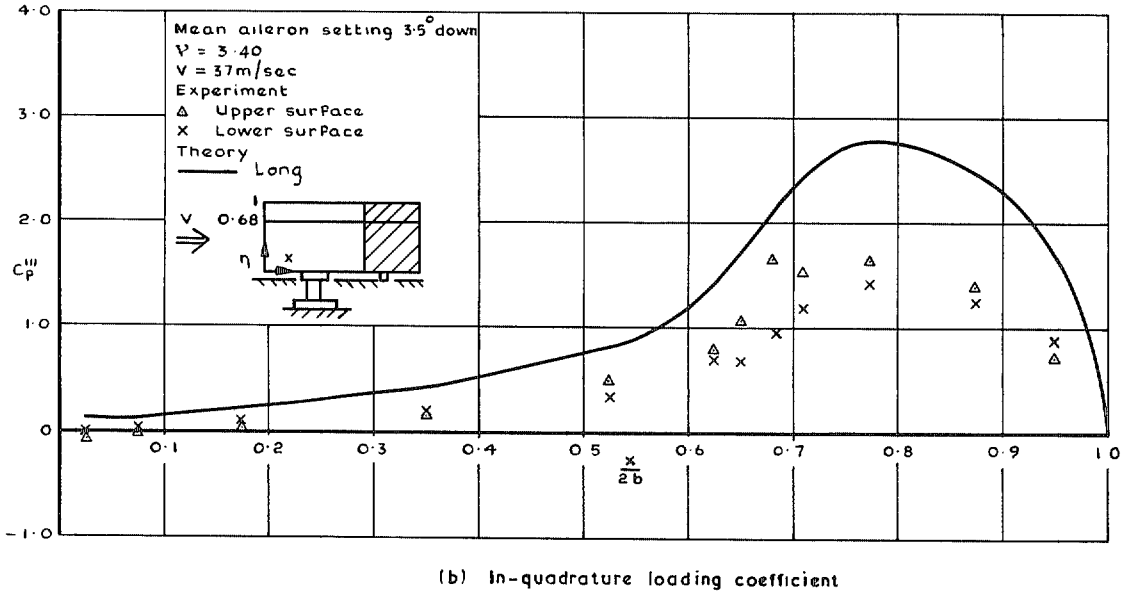

(b) In-quadrature loading coefficient

FIG. 17 (a) and (b). Loading coefficients at $\eta = 0{\cdot}68$—full-span control.

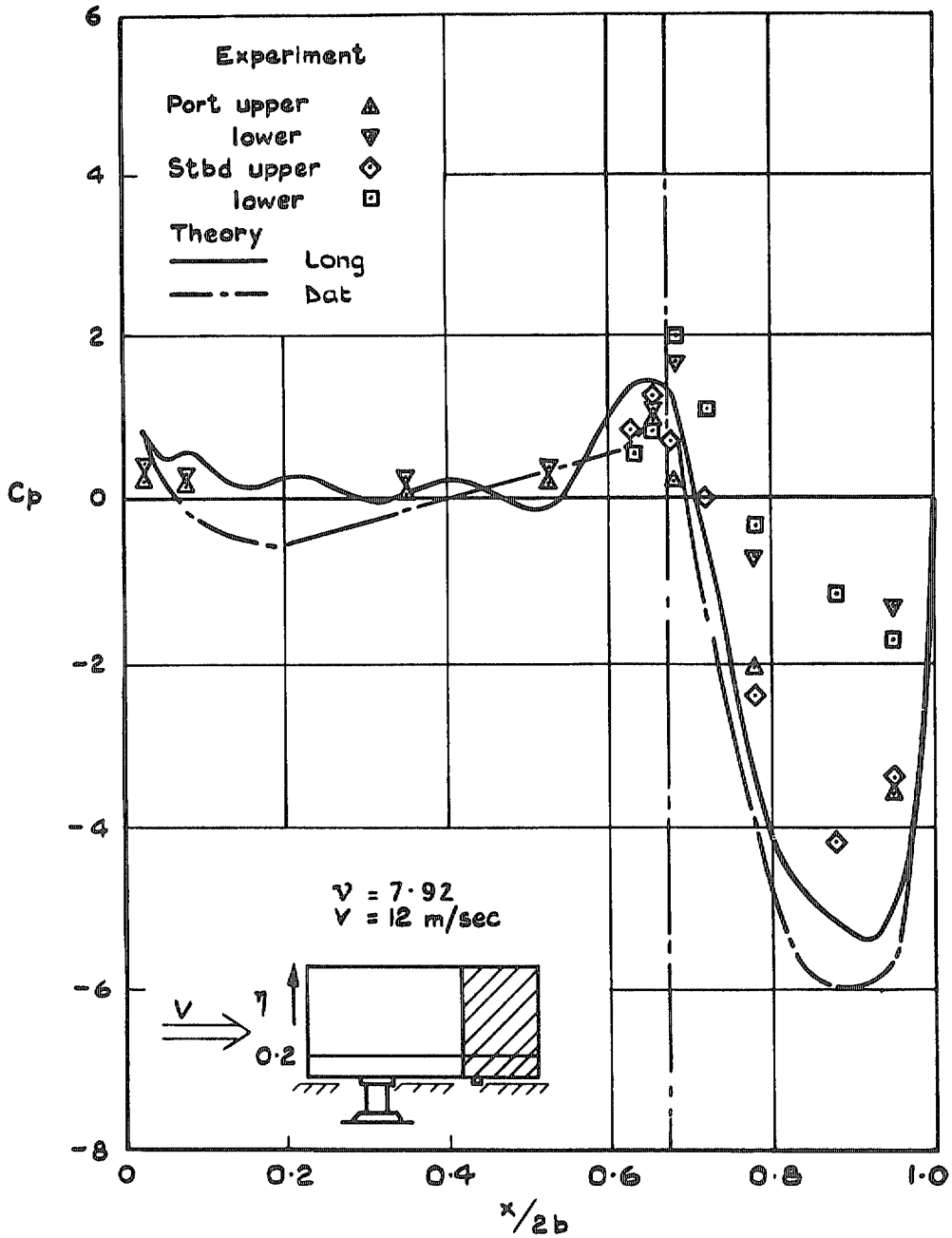

(a) In-phase loading coefficient

FIG. 18 (a) and (b). Loading coefficients at $\eta = 0{\cdot}2$—full-span control.

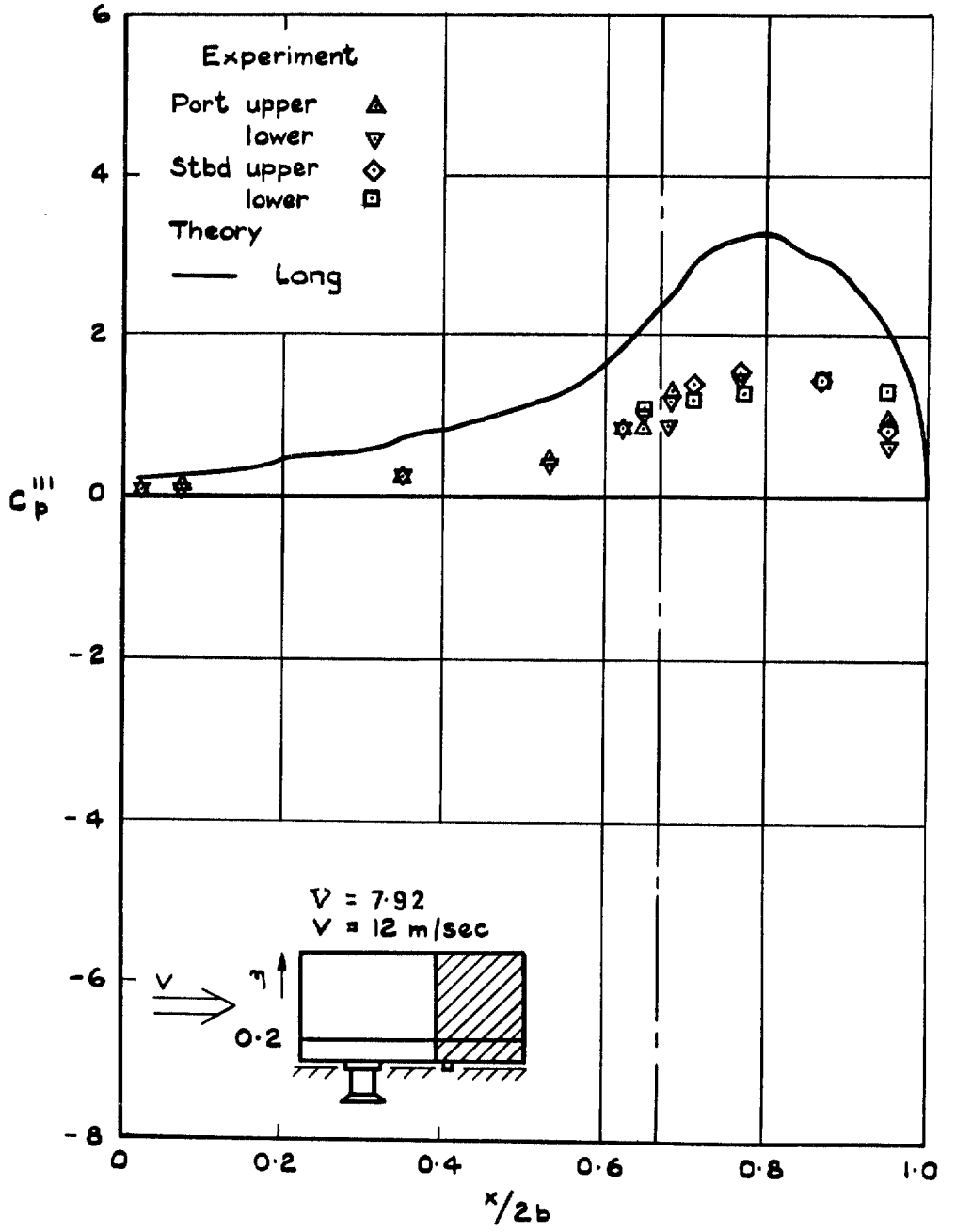

(b) In-quadrature loading coefficient

FIG. 18 continued.

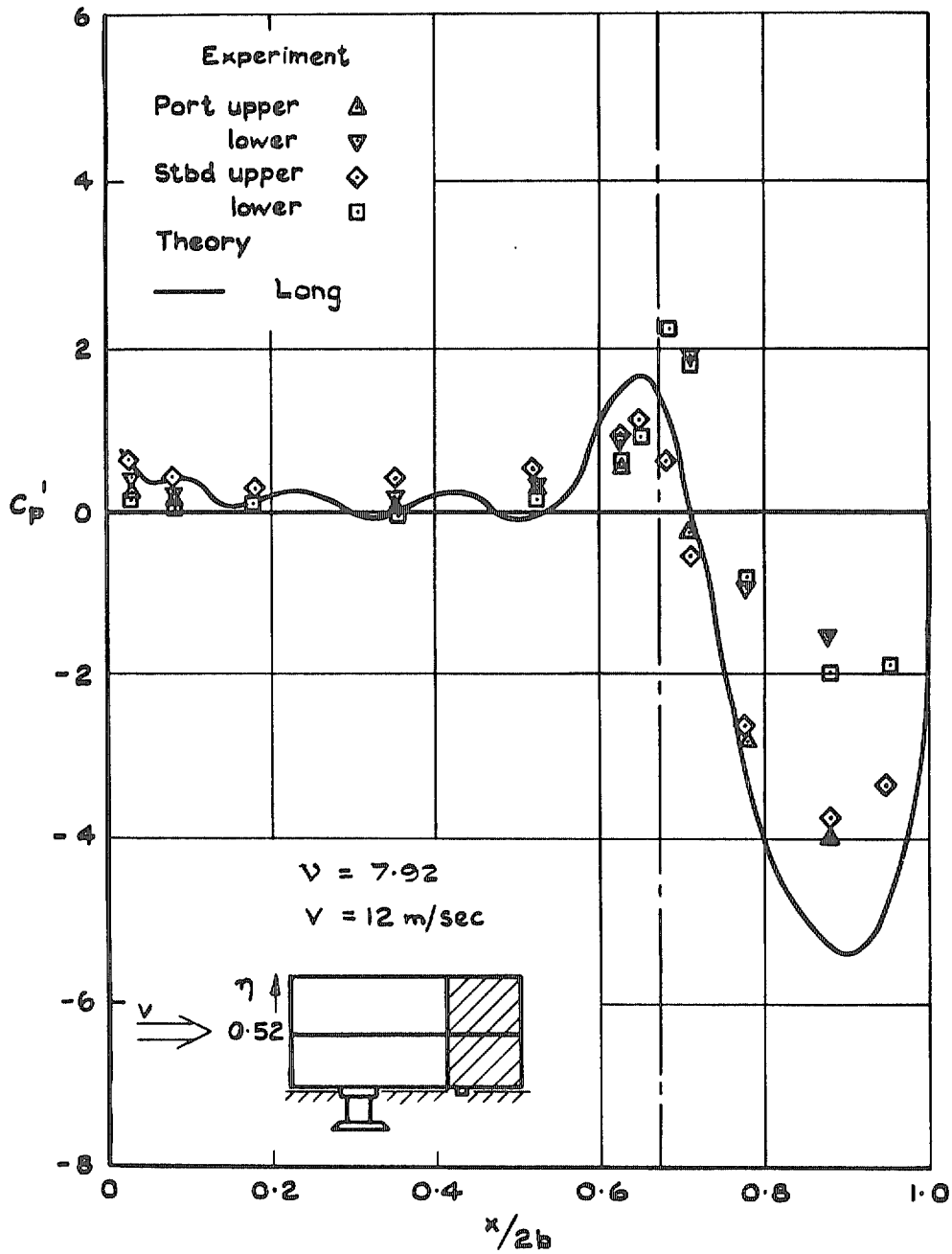

(a) In-phase loading coefficient

FIG. 19 (a) and (b). Loading coefficients at $\eta = 0{\cdot}52$—full-span control.

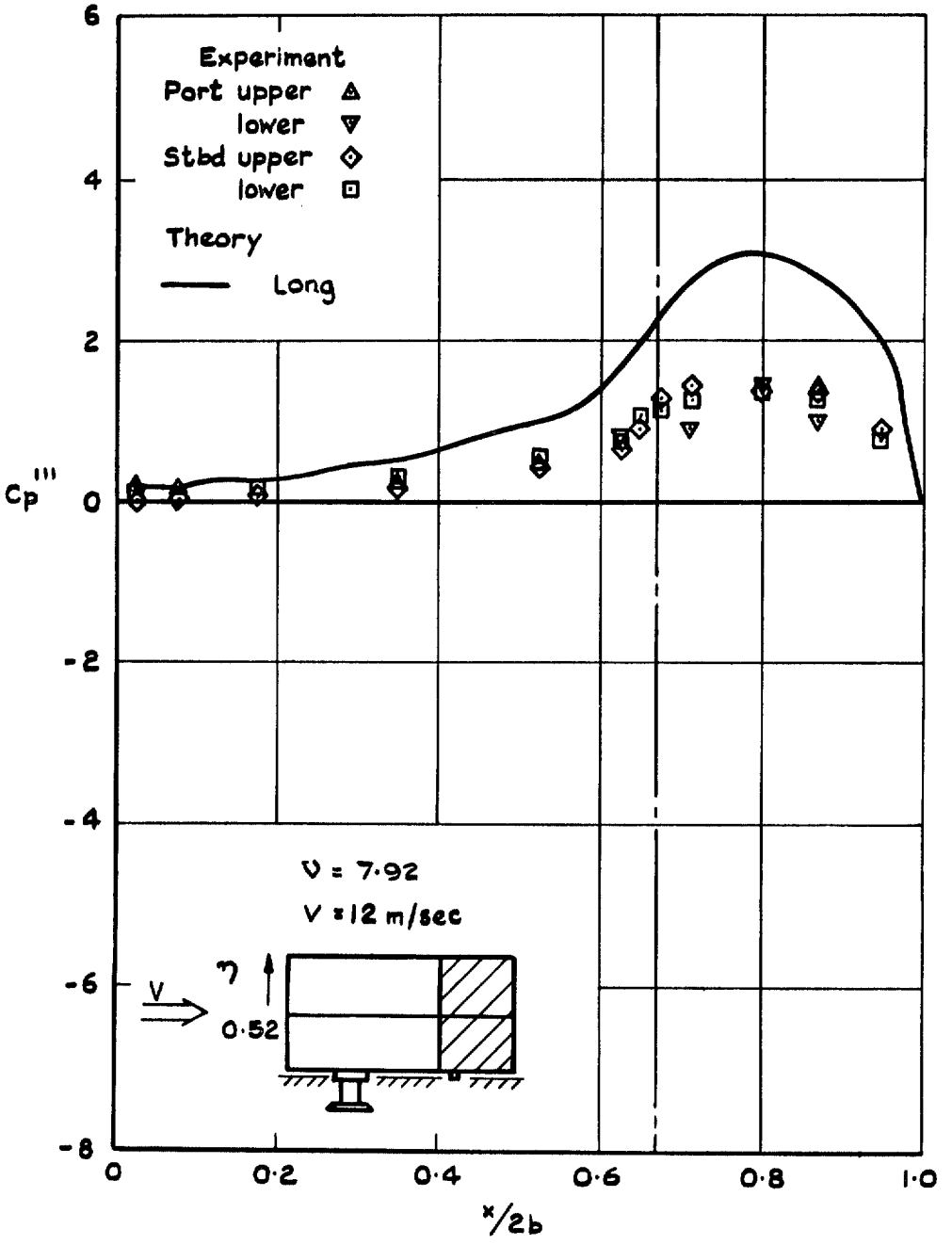

(b) In-quadrature loading coefficient

FIG. 19 continued.

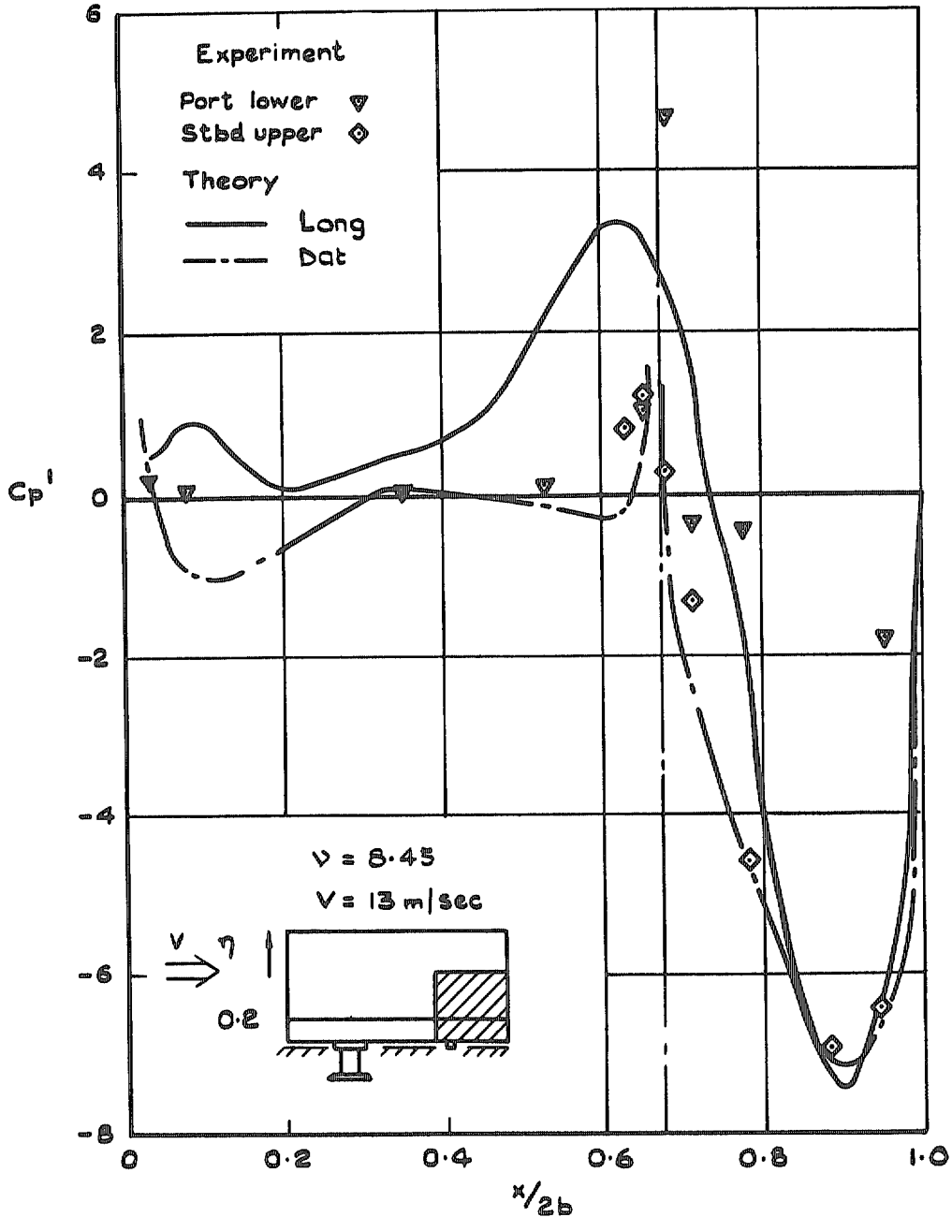

(a) In-phase loading coefficient

FIG. 20 (a) and (b). Loading coefficients at $\eta = 0{\cdot}2$—part-span control.

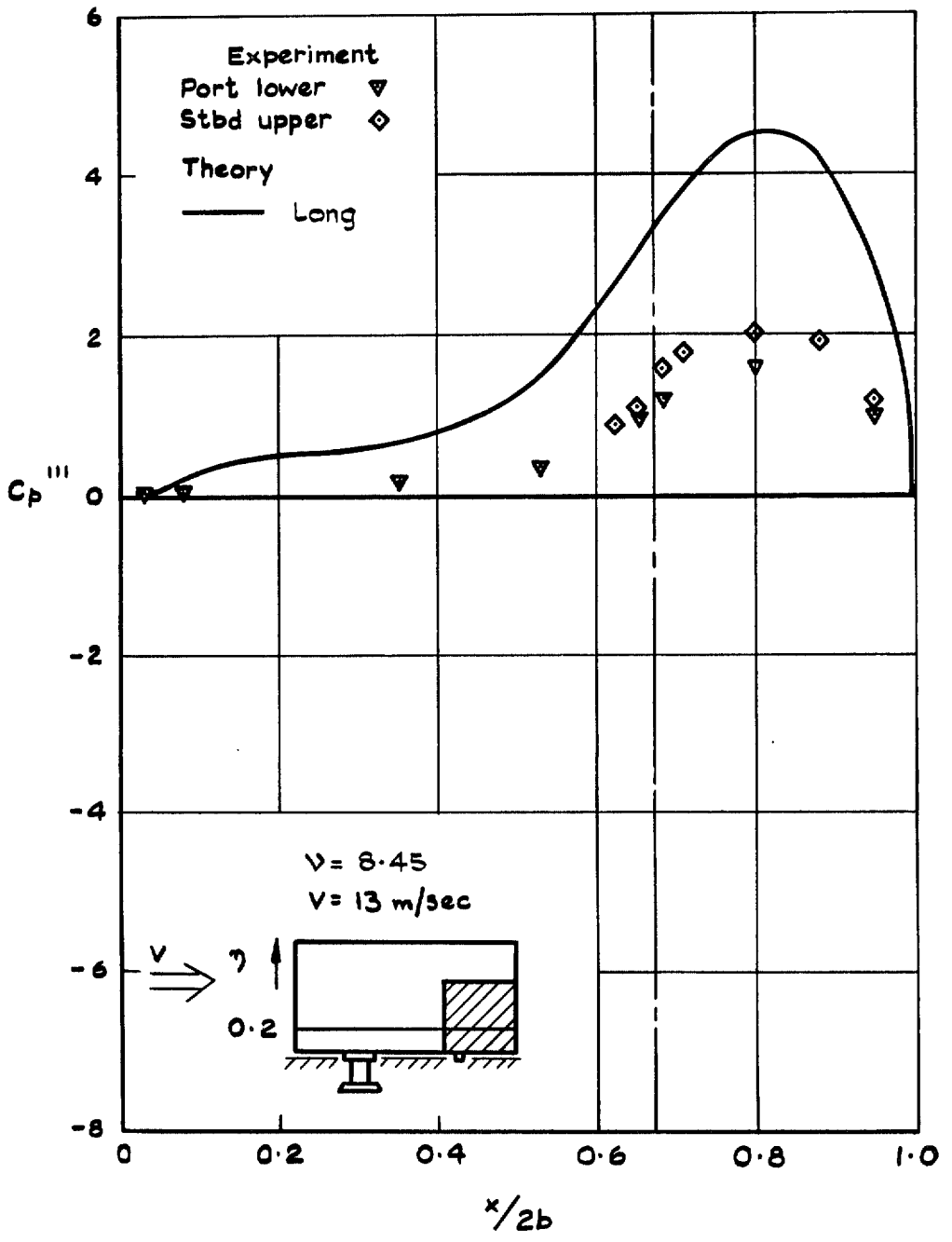

(b) In-quadrature loading coefficient

FIG. 20 continued.

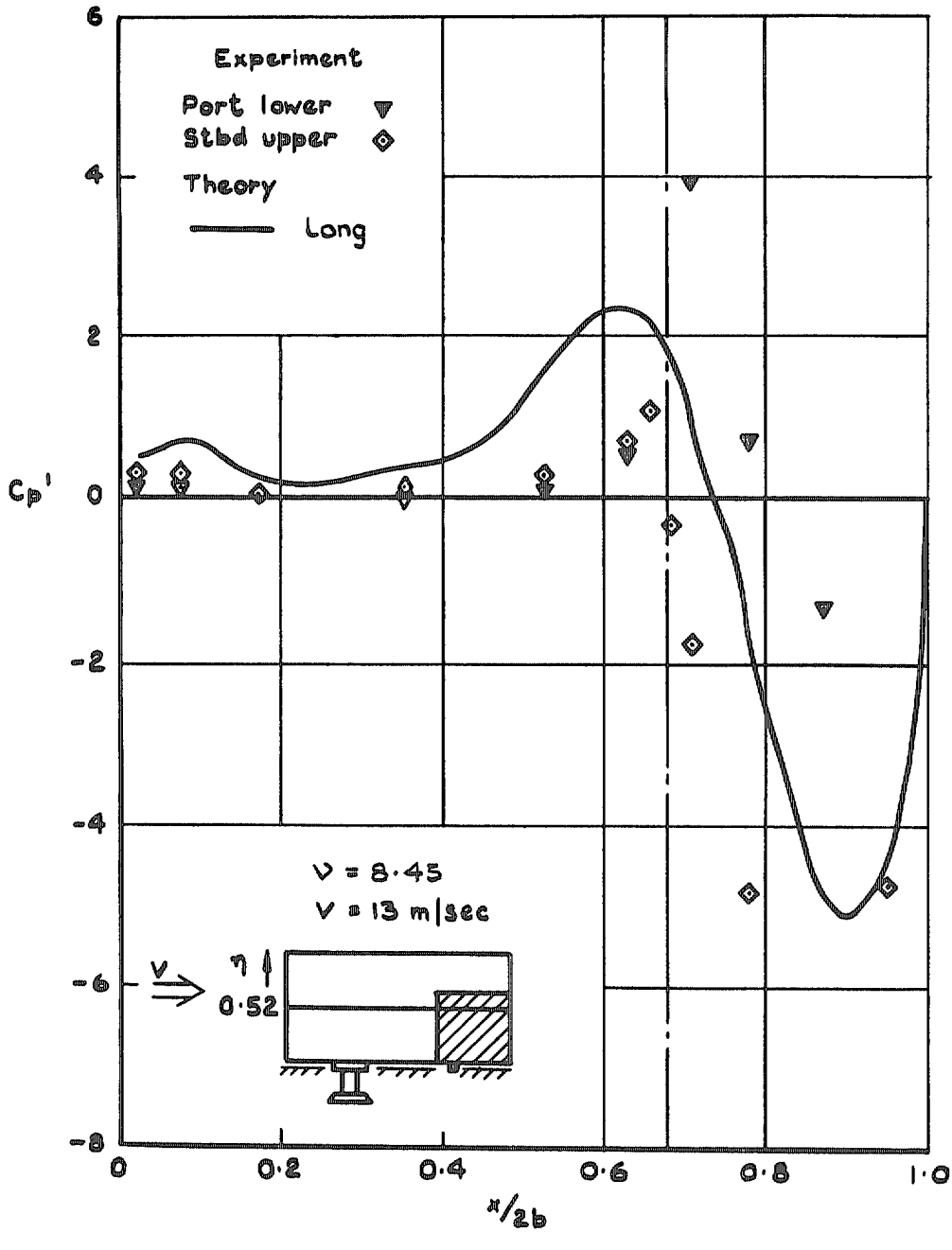

(a) In-phase loading coefficient

FIG. 21 (a) and (b). Loading coefficients at $\eta = 0{\cdot}52$—part-span control.

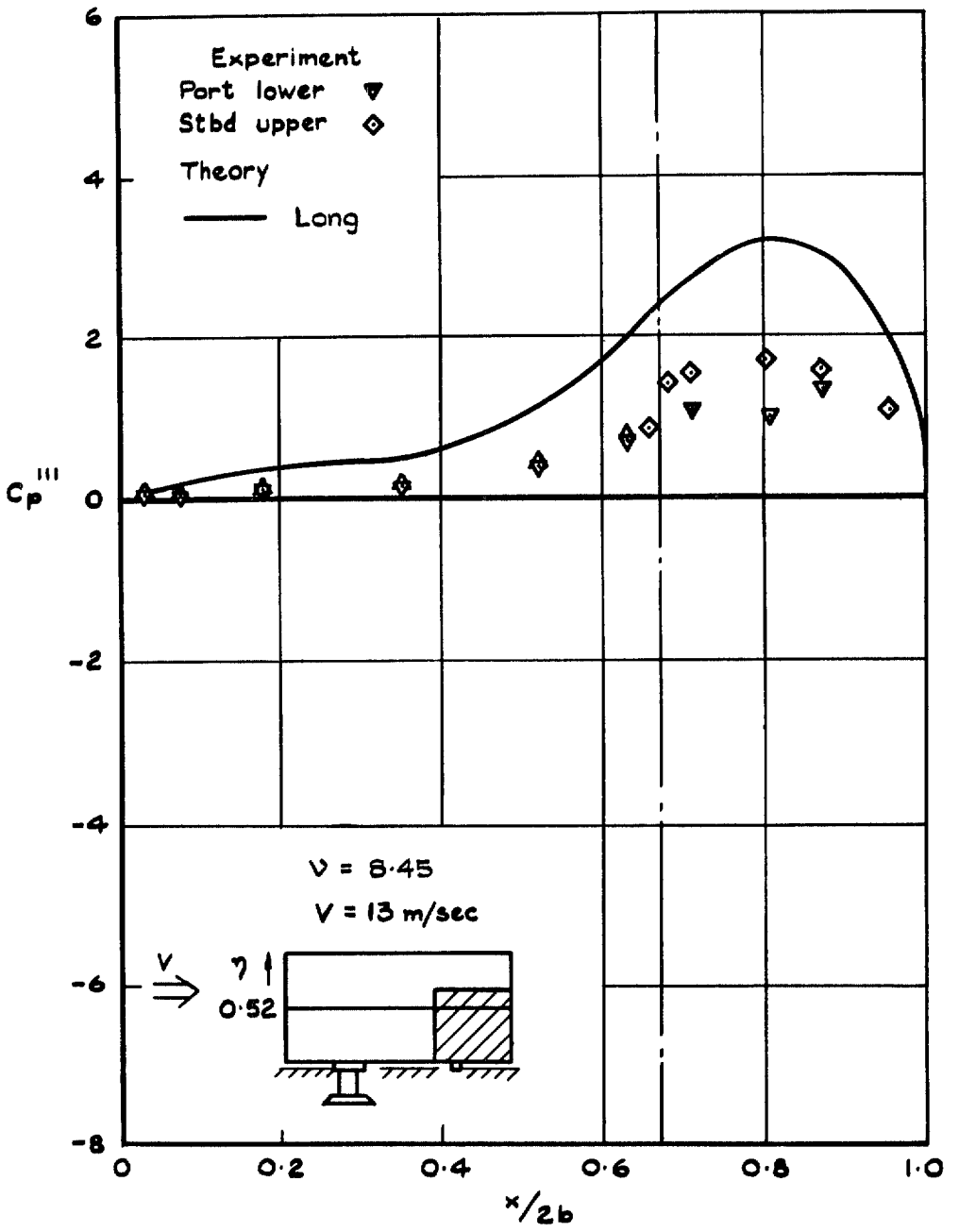

(b) In-quadrature loading coefficient

FIG. 21 continued.

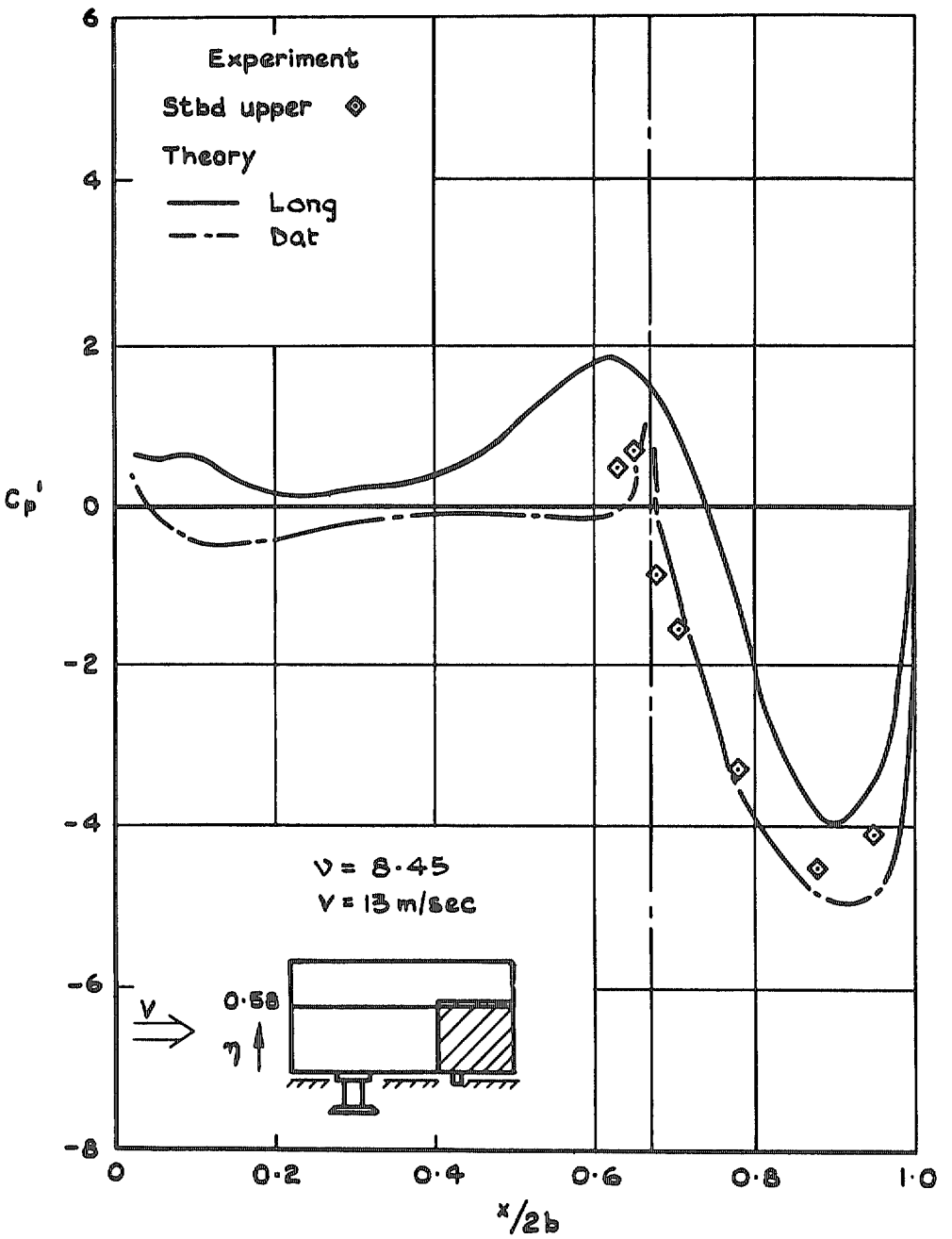

FIG. 22. In-phase loading coefficients at $\eta = 0{\cdot}58$—part-span control.

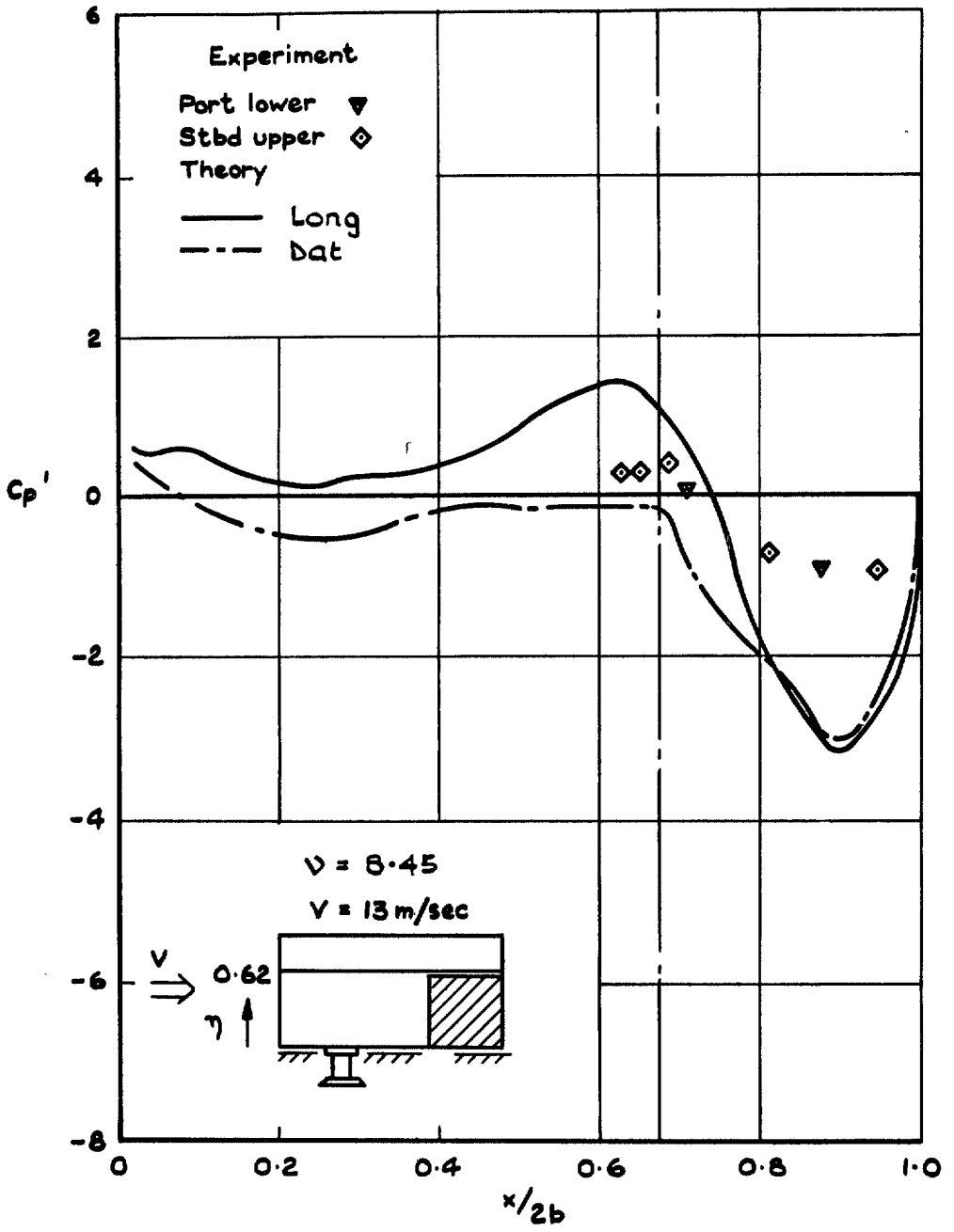

FIG. 23. In-phase loading coefficients at $\eta = 0{\cdot}62$—part-span control.

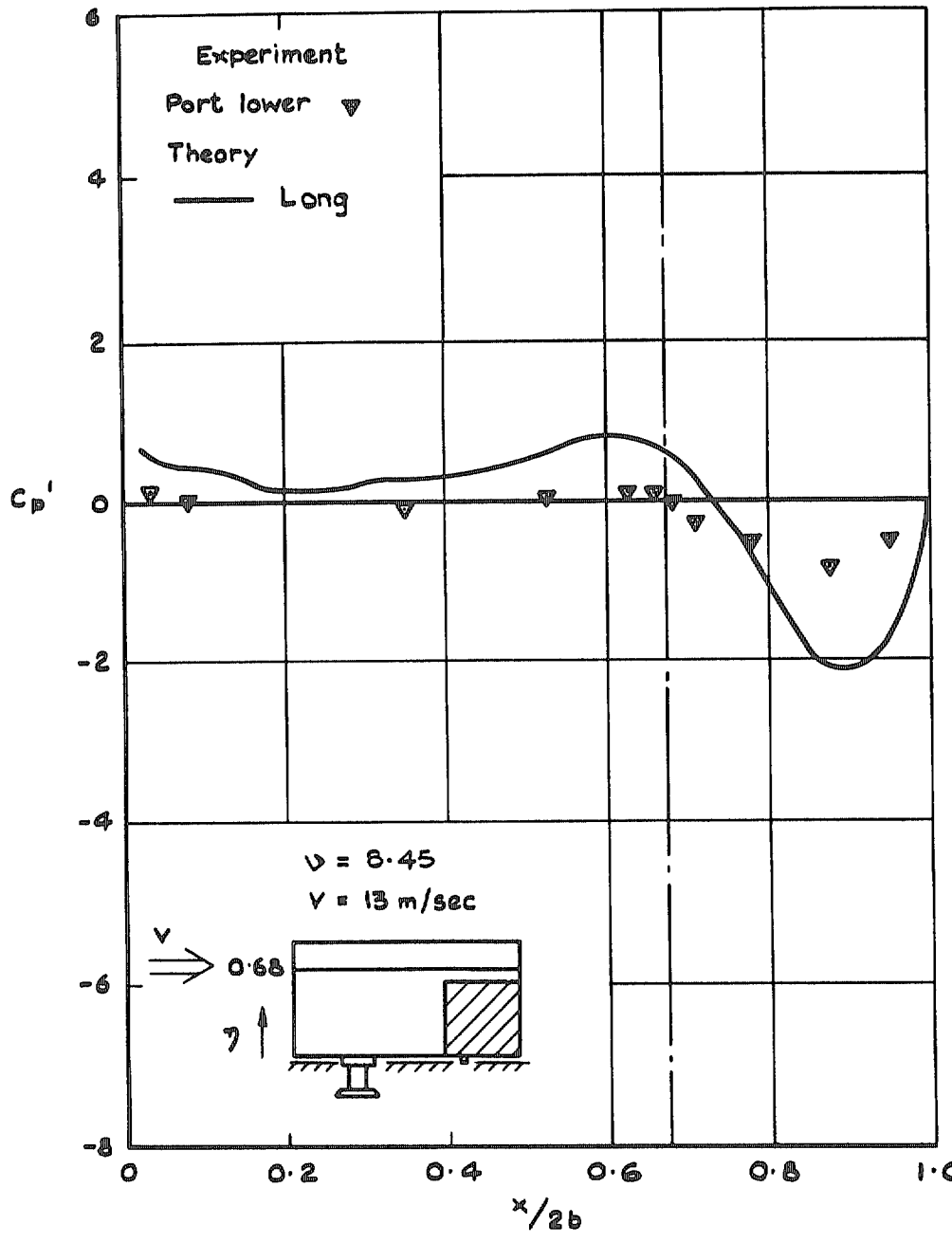

(a) In-phase loading coefficient

FIG. 24 (a) and (b). Loading coefficient at η = 0·68—part-span control.

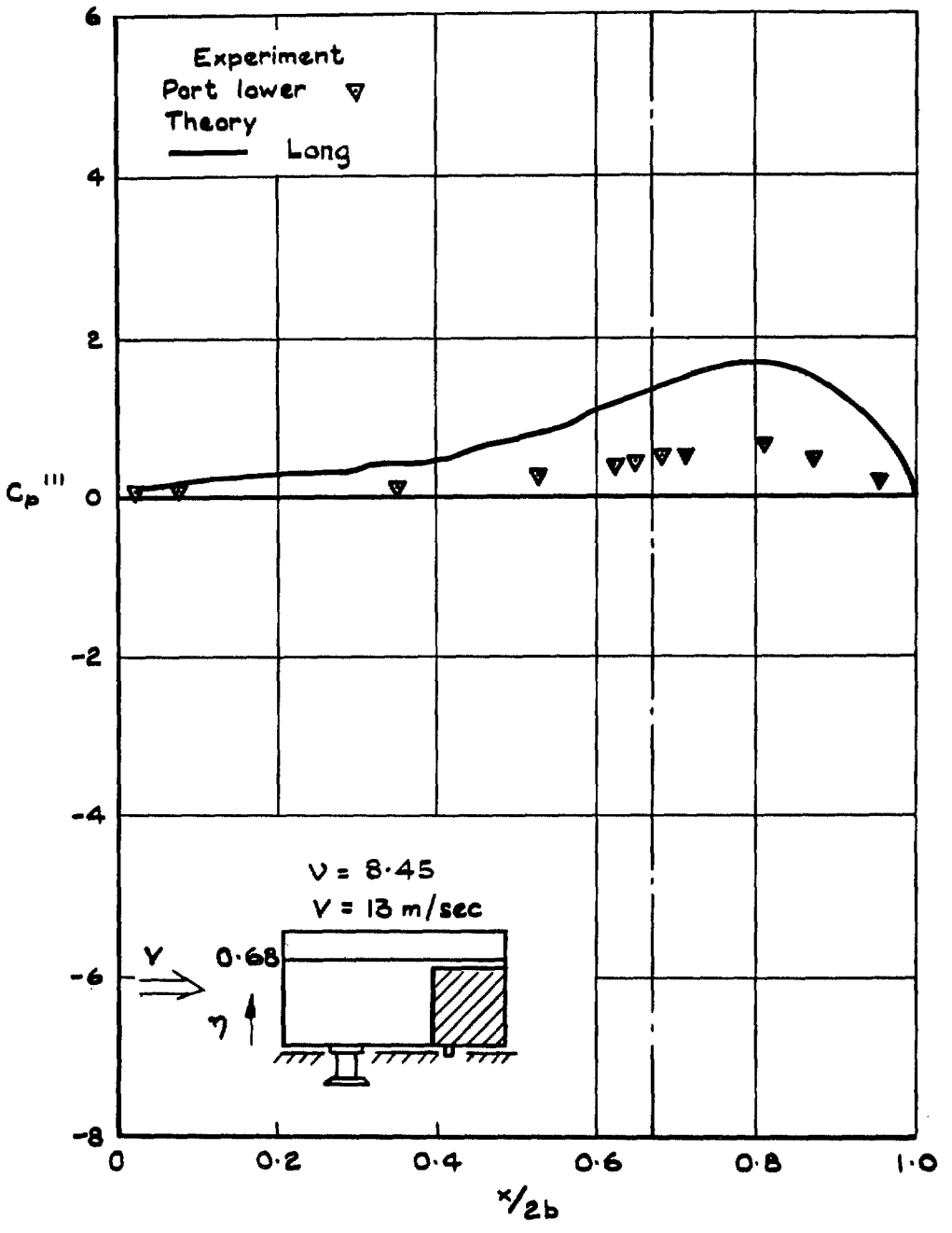

(b) In-quadrature loading coefficient

FIG. 24 continued.

Printed in England for Her Majesty's Stationery Office by J. W. Arrowsmith Ltd., Bristol BS3 2NT
Dd. 505374 K5 3/76

HER MAJESTY'S STATIONERY OFFICE

Government Bookshops

49 High Holborn, London WC1V 6HB
13a Castle Street, Edinburgh EH2 3AR
41 The Hayes, Cardiff CF1 1JW
Brazennose Street, Manchester M60 8AS
Southey House, Wine Street, Bristol BS1 2BQ
258 Broad Street, Birmingham B1 2HE
80 Chichester Street, Belfast BT1 4JY

Government publications are also available through booksellers

ISBN 0 11 470908 4